counts. The lack of a significant association may reflect an indirect, rather than a direct, relationship between *ITPA* genotype and platelet physiology.

Tanaka et al. [12] showed that a *DDRGK1* SNP near the *ITPA* gene, like the *ITPA* SNP, was associated with treatment-induced anemia; moreover, the *DDRGK1* SNP was associated with treatment-induced thrombocytopenia during PEG-IFN/RBV combination therapy. Because a protective *DDRGK1* allele showed linkage with a protective *ITPA* allele in all the patients enrolled in the present study, the association between *DDRGK1* SNP and changes in platelet counts could not be further examined.

In conclusion, an association was found between *ITPA* SNP genotype and treatment-induced anemia during a 4-week course of RBV monotherapy. This RBV-induced anemia may have led to increases in endogenous serum EPO that, in turn, resulted in the stimulation of platelet production. However, the sample size in this study was small; therefore, further investigations are needed to elucidate the effects of RBV on hematopoietic parameters.

# References

1. Lavanchy D. Evolving epidemiology of hepatitis C virus. Clin Microbiol Infect. 2011;17:107–15.
2. Thomas DL, Astemborski J, Rai RM, Anania FA, Schaeffer M, Galai N, et al. The natural history of hepatitis C virus infection: host, viral, and environmental factors. JAMA. 2000;284:450–6.
3. di Iulio J, Ciuffi A, Fitzmaurice K, Kelleher D, Rotger M, Fellay J, et al. Estimating the net contribution of interleukin-28B variation to spontaneous hepatitis C virus clearance. Hepatology. 2011;53:1446–54.
4. Fried MW, Shiffman ML, Reddy KR, Smith C, Marinos G, Goncales FL, et al. Peginterferon alfa-2a plus ribavirin for chronic hepatitis C virus infection. N Engl J Med. 2002;347:975–82.
5. Hadziyannis SJ, Sette H, Morgan TR, Balan V, Diago M, Marcellin P, et al. Peginterferon-alpha2a and ribavirin combination therapy in chronic hepatitis C: a randomized study of treatment duration and ribavirin dose. Ann Intern Med. 2004;140:346–55.
6. Sidwell RW, Huffman JH, Khare GP, Allen LB, Witkowski JT, Robins RK. Broad-spectrum antiviral activity of Virazole: 1-beta-D-ribofuranosyl-1,2,4-triazole-3-carboxamide. Science. 1972;177:705–6.
7. Reddy KR, Shiffman ML, Morgan TR, Zeuzem S, Hadziyannis S, Hamzeh FM, et al. Impact of ribavirin dose reductions in hepatitis C virus genotype 1 patients completing peginterferon alfa-2a/ribavirin treatment. Clin Gastroenterol Hepatol. 2007;5:124–9.
8. Sulkowski MS, Wasserman R, Brooks L, Ball L, Gish R. Changes in haemoglobin during interferon alpha-2b plus ribavirin combination therapy for chronic hepatitis C virus infection. J Viral Hepat. 2004;11:243–50.
9. Tanaka Y, Nishida N, Sugiyama M, Kurosaki M, Matsuura K, Sakamoto N, et al. Genome-wide association of IL28B with response to pegylated interferon-alpha and ribavirin therapy for chronic hepatitis C. Nat Genet. 2009;41:1105–9.
10. Fellay J, Thompson AJ, Ge D, Gumbs C, Urban TJ, Shianna K, et al. ITPA gene variants protect against anaemia in patients treated for chronic hepatitis C. Nature. 2010;464:405–8.
11. Ochi H, Maekawa T, Abe H, Hayashida Y, Nakano R, Kubo M, et al. ITPA polymorphism affects ribavirin-induced anemia and outcomes of therapy—a genome-wide study of Japanese HCV virus patients. Gastroenterology. 2010;139:1190–7.
12. Tanaka Y, Kurosaki M, Nishida N, Sugiyama M, Matsuura K, Sakamoto N, et al. Genome-wide association study identified ITPA/DDRGK1 variants reflecting thrombocytopenia in pegylated interferon and ribavirin therapy for chronic hepatitis C. Hum Mol Genet. 2011;20:3507–16.
13. Homma M, Jayewardene AL, Gambertoglio J, Aweeka F. High-performance liquid chromatographic determination of ribavirin in whole blood to assess disposition in erythrocytes. Antimicrob Agents Chemother. 1999;43:2716–9.
14. Pawlotsky JM, Dahari H, Neumann AU, Hézode C, Germanidis G, Lonjon I, et al. Antiviral action of ribavirin in chronic hepatitis C. Gastroenterology. 2004;126:703–14.
15. Hézode C, Forestier N, Dusheiko G, Ferenci P, Pol S, Goeser T, et al. Telaprevir and peginterferon with or without ribavirin for chronic HCV infection. N Engl J Med. 2009;360:1839–50.
16. Canonico PG, Kastello MD, Cosgriff TM, Donovan JC, Ross PE, Spears CT, et al. Hematological and bone marrow effects of ribavirin in rhesus monkeys. Toxicol Appl Pharmacol. 1984;74:163–72.
17. Streja E, Kovesdy CP, Greenland S, Kopple JD, McAllister CJ, Nissenson AR, et al. Erythropoietin, iron depletion, and relative thrombocytosis: a possible explanation for hemoglobin-survival paradox in hemodialysis. Am J Kidney Dis. 2008;52:727–36.
18. Homoncik M, Jilma-Stohlawetz P, Schmid M, Ferlitsch A, Peck-Radosavljevic M. Erythropoietin increases platelet reactivity and platelet counts in patients with alcoholic liver cirrhosis: a randomized, double-blind, placebo-controlled study. Aliment Pharmacol Ther. 2004;20:437–43.
19. Dessypris EN, Gleaton JH, Armstrong OL. Effect of human recombinant erythropoietin on human marrow megakaryocyte colony formation in vitro. Br J Haematol. 1987;65:265–9.
20. Vaziri ND. Thrombocytosis in EPO-treated dialysis patients may be mediated by EPO rather than iron deficiency. Am J Kidney Dis. 2009;53:733–6.
21. Bilic E. Amino acid sequence homology of thrombopoietin and erythropoietin may explain thrombocytosis in children with iron deficiency anemia. J Pediatr Hematol Oncol. 2003;25:675–6.
22. Tekin D, Yavuzer S, Tekin M, Akar N, Cin S. Possible effects of antioxidant status on increased platelet aggregation in childhood iron-deficiency anemia. Pediatr Int. 2001;43:74–7.
23. Youdim MB, Woods HF, Mitchell B, Grahame-Smith DG, Callender S. Human platelet monoamine oxidase activity in iron-deficiency anaemia. Clin Sci Mol Med. 1975;48:289–95.
24. Schmid M, Kreil A, Jessner W, Homoncik M, Datz C, Gangl A, et al. Suppression of haematopoiesis during therapy of chronic hepatitis C with different interferon alpha mono and combination therapy regimens. Gut. 2005;54:1014–20.
25. De Franceschi L, Fattovich G, Turrini F, Ayi K, Brugnara C, Manzato F, et al. Hemolytic anemia induced by ribavirin therapy in patients with chronic hepatitis C virus infection: role of membrane oxidative damage. Hepatology. 2000;31:997–1004.
26. Vanderheiden BS. Genetic studies of human erythrocyte inosine triphosphatase. Biochem Genet. 1969;3:289–97.

# Hepatitis C Virus NS4B Protein Targets STING and Abrogates RIG-I–Mediated Type I Interferon-Dependent Innate Immunity

Sayuri Nitta,[1*] Naoya Sakamoto,[1,2,6*] Mina Nakagawa,[1,2] Sei Kakinuma,[1,2] Kako Mishima,[1]
Akiko Kusano-Kitazume,[1] Kei Kiyohashi,[1] Miyako Murakawa,[1] Yuki Nishimura-Sakurai,[1] Seishin Azuma,[1]
Megumi Tasaka-Fujita,[1] Yasuhiro Asahina,[1,2] Mitsutoshi Yoneyama,[3] Takashi Fujita,[4,5] and Mamoru Watanabe[1]

Hepatitis C virus (HCV) infection blocks cellular interferon (IFN)-mediated antiviral signaling through cleavage of Cardif by HCV-NS3/4A serine protease. Like NS3/4A, NS4B protein strongly blocks IFN-$\beta$ production signaling mediated by retinoic acid–inducible gene I (RIG-I); however, the underlying molecular mechanisms are not well understood. Recently, the stimulator of interferon genes (STING) was identified as an activator of RIG-I signaling. STING possesses a structural homology domain with flaviviral NS4B, which suggests a direct protein-protein interaction. In the present study, we investigated the molecular mechanisms by which NS4B targets RIG-I–induced and STING-mediated IFN-$\beta$ production signaling. IFN-$\beta$ promoter reporter assay showed that IFN-$\beta$ promoter activation induced by RIG-I or Cardif was significantly suppressed by both NS4B and NS3/4A, whereas STING-induced IFN-$\beta$ activation was suppressed by NS4B but not by NS3/4A, suggesting that NS4B had a distinct point of interaction. Immunostaining showed that STING colocalized with NS4B in the endoplasmic reticulum. Immunoprecipitation and bimolecular fluorescence complementation (BiFC) assays demonstrated that NS4B specifically bound STING. Intriguingly, NS4B expression blocked the protein interaction between STING and Cardif, which is required for robust IFN-$\beta$ activation. NS4B truncation assays showed that its N terminus, containing the STING homology domain, was necessary for the suppression of IFN-$\beta$ promoter activation. NS4B suppressed residual IFN-$\beta$ activation by an NS3/4A-cleaved Cardif (Cardif1-508), suggesting that NS3/4A and NS4B may cooperate in the blockade of IFN-$\beta$ production. *Conclusion*: NS4B suppresses RIG-I–mediated IFN-$\beta$ production signaling through a direct protein interaction with STING. Disruption of that interaction may restore cellular antiviral responses and may constitute a novel therapeutic strategy for the eradication of HCV. (HEPATOLOGY 2013;57:46-58)

Type I interferon (IFN) plays a central role in eliminating hepatitis C virus (HCV) both under physiological conditions and when used as a therapeutic intervention.[1-3] In experimental acute-resolving HCV infection in chimpanzees, numerous IFN-related genes are expressed during clinical course of infection.[4] Viruses are recognized by cellular innate immune receptors, such as toll-like receptors, and a family of RIG-I–like receptors, such as retinoic-acid-inducible gene I (RIG-I) and melanoma-differentiation-associated gene 5 (MDA-5); host antiviral responses are then activated, resulting in the

46

production of cytokines such as type I and type III IFNs.[5] RIG-I is activated through recognition of short double-strand RNA (dsRNA) or triphosphate at the 5' end of dsRNA as pathogen-associated molecular patterns,[6,7] forming a homo-oligomer that binds with the caspase recruitment domain (CARD) of Cardif (also known as MAVS, VISA, or IPS-1).[8-11] Cardif subsequently recruits TANK binding kinase 1 (TBK1) and IκB kinase ε (IKKε) kinases, which catalyze phosphorylation and activation of IFN regulatory factor-3 (IRF-3).[12] Activation of TBK1 and IKKε results in the phosphorylation of IRF-3 or IRF-7, translocation to the nucleus, and induction of IFN-$\beta$ mRNA transcription.

Several HCV proteins can block host cellular antiviral responses. HCV core protein blocks IFN signaling by interacting with signal transducer and activator of transcription protein-1 (STAT1).[13] The core protein also induces expression of suppressor of cytokine signaling-1 (SOCS1) and SOCS3, and blocks Janus kinase–STAT signaling.[14,15] A well-elucidated immune evasion strategy of HCV involves NS3/4A serine protease and its ability to inhibit host IFN signal pathways. Gale and colleagues[11,16,17] revealed that NS3/4A protease cleaves Cardif at Cys-508 resulting in dislocation of Cardif from mitochondria, and blocks downstream signaling of IFN-$\beta$ production. On the other hand, Baril et al.[18] reported that Cardif was still able to form a homo-oligomer and to activate downstream IFN production signaling despite delocalization from the mitochondria. These reports suggest that homo-oligomerization of Cardif, and not mitochondrial anchorage, is essential for the activation of downstream IFN signaling and that other virus-derived molecules may cooperate with NS3/4A to abrogate the signaling of IFN production.

We reported previously that HCV-NS4B, as well as NS3/4A, inhibited RIG-I and Cardif-mediated interferon-stimulated response element (ISRE) activation, while TBK1- and IKKε-mediated ISRE activation were not suppressed.[19] These results indicate that NS4B suppresses IFN production signaling by targeting Cardif or other unknown signaling molecules between the level of Cardif and TBK1/IKKε.

Recently, a stimulator of interferon genes (STING, also known as MITA/ERIS/MPYS/TMEM173) was identified as a positive regulator of RIG-I–mediated IFN-$\beta$ signaling.[20-23] STING is a 42-kDa protein localized predominantly in the endoplasmic reticulum (ER) that binds RIG-I, Cardif, TBK1, and IKKε. STING is thought to act as a scaffold for Cardif/TBK1/IRF-3 complex upon viral infection.[22] It has been reported that NS4B of yellow fever virus, which is a member of the flaviviridae family of viruses, inhibits STING activation probably through a direct molecular interaction.[24] These reports have led us postulate that HCV-NS4B may also inhibit RIG-I dependent IFN signaling through association with STING.

In the present study, we further investigated the molecular mechanisms by which HCV-NS4B protein inhibits RIG-I–mediated IFN expression signaling. We demonstrated that HCV-NS4B specifically binds STING, blocks the molecular interaction between STING and Cardif, and suppresses the RIG-I–like receptor–induced activation of IFN-$\beta$ production signaling.

## Materials and Methods

*Plasmids.* The ΔRIG-I and RIG-IKA plasmids express constitutively active and inactive RIG-I, respectively.[5] Full-length Cardif (Cardif) and CARD-truncated Cardif (ΔCARD) plasmids were provided by J. Tschopp.[11] Plasmids expressing STING were provided by G. N. Barber.[20] Plasmids expressing HCV NS3/4A, NS4B, and truncated NS4B have been described.[25] Plasmid pIFN$\beta$-Fluc was provided by R. Lin.[26]

*Cell Culture.* HEK293T and Huh7 cells were maintained in Dulbecco's modified minimal essential medium (Sigma) supplemented with 2 mM L-glutamine and 10% fetal calf serum at 37°C with 5% $CO_2$.

*HCV Replicon Constructs and HCV-JFH1 Cell Culture.* An HCV subgenomic replicon plasmid, pRep-Feo, expressed fusion protein of firefly luciferase and neomycin phosphotransferase.[27,28] Huh7 cells were transfected by Rep-Feo RNA, cultured in the presence of 500 μg/mL of G418, and a cell line that stably expressed Feo replicon was established. For HCV cell culture, the HCV-JFH1 strain was used.[29,30]

*Antibodies.* Antibodies used were anti–IRF-3 (FL-425, Santa Cruz Biotechnology), anti-HA (Invitrogen), anti-myc (Invitrogen), mouse anti-PDI (Abcam),

View this article online at wileyonlinelibrary.com.
Potential conflict of interest: Nothing to report.
Additional Supporting Information may be found in the online version of this article.

rabbit anti-PDI (Enzo Life Science), anti-Flag (Sigma Aldrich), anti-Cardif (Enzo Life Science), anti-phospho–IRF-3 (Ser396, Millipore), anti-monomeric Kusabira-Green C- or N-terminal fragment (MBL), and anti-FACL4 (Abgent).

*Luciferase Reporter Assay.* IFN-$\beta$ reporter assays were performed as described.[19,31] The plasmids pIFN-$\beta$-Fluc and pRL-CMV were cotransfected with NS3/4A or NS4B, and $\Delta$RIG-I, Cardif, STING or poly(deoxyadenylic-deoxythymidylic) acid [poly(dA:dT)] (Invivogen). RIG-IKA, $\Delta$CARD, and pcDNA3.1, respectively, were used as controls. Luciferase assays were performed 24 hours after transfection by using a 1420 Multilabel Counter (ARVO MX PerkinElmer) and Dual Luciferase Assay System (Promega). Assays were performed in triplicate, and the results are expressed as the mean $\pm$ SD.

*Immunoblotting.* Preparation of total cell lysates was performed as described.[19,28] Protein was separated using NuPAGE 4%-12% Bis/Tris gels (Invitrogen) and blotted onto an Immobilon polyvinylidene difluoride membrane. The membrane was immunoblotted with primary followed by secondary antibody, and protein was detected by chemiluminescence.

*Immunoprecipitation Assay.* HEK-293T or Huh7 cells were transfected with plasmids as indicated. Twenty-four hours after transfection, cellular proteins were harvested and immunoprecipitation assays were performed using an Immunoprecipitation Kit according to the manufacturer's protocol (Roche Applied Science). The immunoprecipitated proteins were analyzed by immunoblotting.

*Indirect Immunofluorescence Assay.* Cells seeded onto tissue culture chamber slides were transfected with plasmids as indicated. Twenty-four hours after transfection, the cells were fixed with cold acetone and incubated with primary antibody and subsequently with Alexa488- or Alexa568-labeled secondary antibodies. Mitochondria were stained by MitoTracker (Invitrogen). Cells were visualized using a confocal laser microscope (Fluoview FV10, Olympus).

*BiFC Assay.* Expression plasmids of NS4B, Cardif, or STING that was fused with N- or C-terminally truncated monomeric Kusabira-Green (mKG) were constructed by inserting polymerase chain reaction–amplified fragments encoding NS4B, Cardif, or STING, respectively, inserted into fragmented mKG vector (Coral Hue Fluo-Chase Kit; MBL). HEK293T cells were transfected with a complementary pair of mKG fusion plasmids. Twenty-four hours after transfection, fluorescence-positive cells were detected and counted by flow cytometry, or observed by confocal laser microscopy.

*Small Interfering RNA Assay.* Nucleotide sequences of STING-targeted small interfering RNAs (siRNAs) were as follows: (1) 5′-gcaacagcatctatgagcttctggagaac-3′, (2) 5′- gtgcagtgagccagcggctgtatattctc;-3′, (3) 5′-gctggcat ggtcatattacatcggatatc-3′.[22] Stealth RNAi Negative Control Duplex (Medium GC Duplex, Invitrogen) was used. Forty-eight hours after siRNA transfection, expression levels of STING were detected by immunoblotting.

*Statistical Analyses.* Statistical analyses were performed using unpaired, two-tailed Student $t$ test. $P < 0.05$ were considered to be statistically significant.

## Results

*NS4B Suppressed RIG-I, Cardif, and STING-Mediated Activation of IFN-$\beta$ Expression Signaling.* First, we performed a reporter assay using a luciferase reporter plasmid regulated by native IFN-$\beta$ promoter. Consistent with our previous study,[19] overexpression of NS4B, as well as NS3/4A, inhibited the IFN-$\beta$ promoter activation that was induced by $\Delta$RIG-I and Cardif, respectively (Fig. 1A). We next studied whether NS4B targets STING and inhibits RIG-I pathway–mediated activation of IFN-$\beta$ production. Expression of NS4B protein significantly suppressed STING-mediated activation of the IFN-$\beta$ promoter reporter, whereas expression of NS3/4A showed no effect on STING-induced IFN-$\beta$ promoter activity (Fig. 1A). To study whether NS4B blocks the STING-mediated DNA-sensing pathway, we performed a reporter assay using a luciferase reporter plasmid cotransfection with poly(dA:dT), which is a synthetic analog of B-DNA and has been reported to induce STING-mediated IFN-$\beta$ production and NS4B. NS4B significantly blocked poly(dA:dT)-induced IFN-$\beta$ promoter activation, suggesting that NS4B may block STING signaling in the DNA-sensing pathway (Fig. 1A).

Activation of RIG-I signaling induces phosphorylation of IRF-3, which is a hallmark of IRF-3 activation.[32] Thus, we examined the effects of NS3/4A and NS4B expression on phosphorylation of IRF-3 by immunoblotting analysis. As shown in Fig. 1B, overexpression of $\Delta$RIG-I, Cardif, or STING in HEK293T cells increased levels of phosphorylated IRF-3 (pIRF-3). Expression of NS4B impaired the IRF-3 phosphorylation that was induced by $\Delta$RIG-I, Cardif, or STING. NS3/4A also blocked production of pIRF-3 induced by $\Delta$RIG-I or Cardif. Intriguingly, NS3/4A did not block STING-induced pIRF-3 production. These results demonstrate that both NS3/4A and
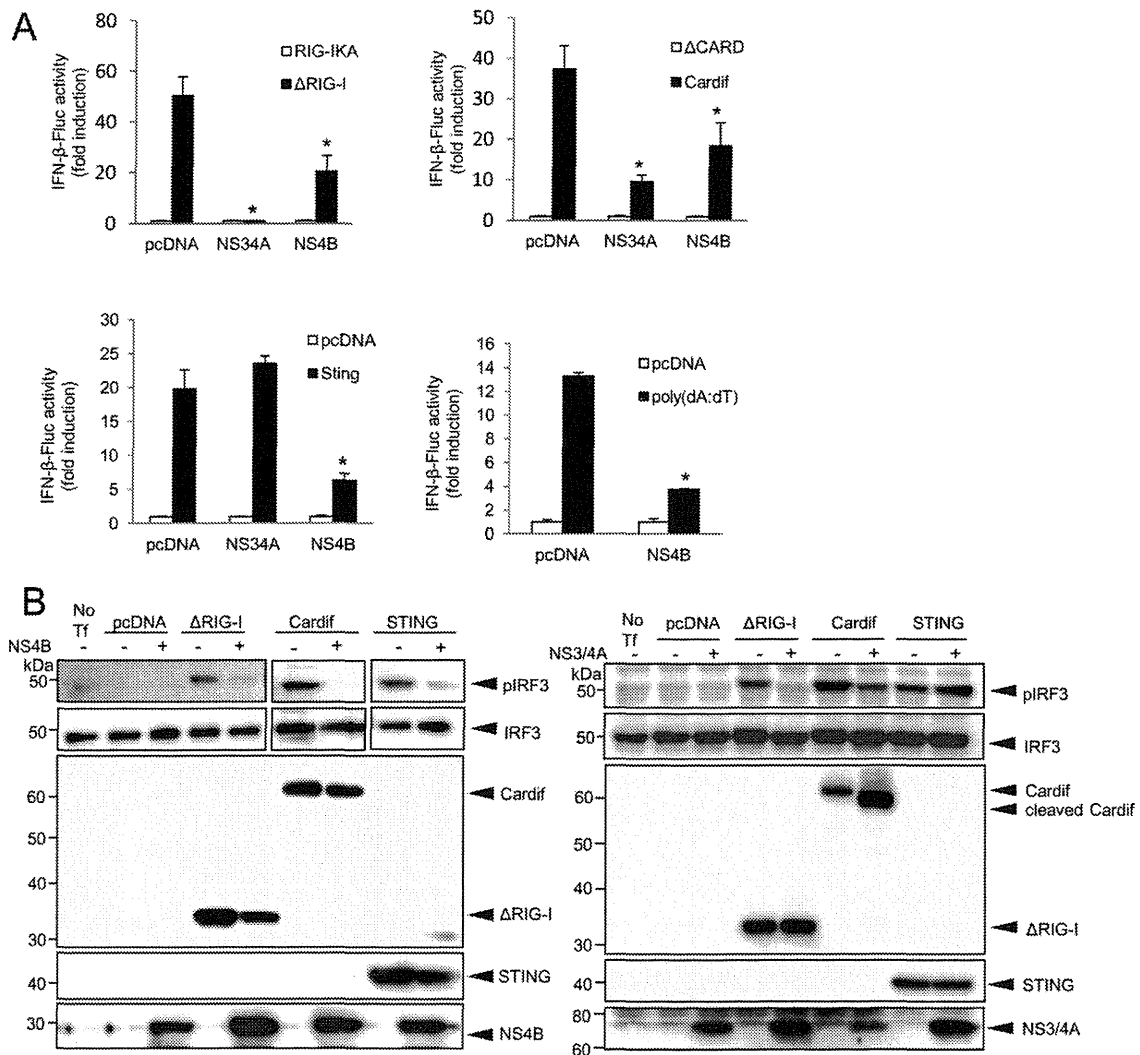
Fig. 1. NS4B suppressed IFN-$\beta$ signaling mediated by RIG-I, Cardif, or STING. (A) Plasmids expressing $\Delta$RIG-I, Cardif, or STING or poly(dA:dT) as well as NS3/4A or NS4B were cotransfected with pIFN-$\beta$-Fluc and pRL-CMV into HEK293T cells. After 24 hours, dual luciferase assays were performed. Plasmids expressing RIG-IKA, $\Delta$CARD, or an empty plasmid (pcDNA) were used as a corresponding negative control. The experiments were performed more than three times and yielded consistent results. The y axis indicates relative IFN-$\beta$-Fluc activity. Assays were performed in triplicate and error bars indicate mean $\pm$ SD. *$P < 0.05$. (B) HEK293T cells were cotransfected with indicated plasmids. On the day after transfection, the cells were lysed and immunoblot analyses were performed. No Tf, transfection-negative controls. pIRF-3 and IRF-3, phosphorylated and total IRF-3, respectively.

NS4B suppress RIG-I–mediated IFN-$\beta$ production, but they do so by targeting different molecules in the signaling pathway.

*Subcellular Localization of NS4B, Cardif, and STING.* We next studied the subcellular localization of NS4B following its overexpression and measured the colocalization of NS4B with Cardif and STING in both HEK293T cells and Huh7 cells by indirect immunofluorescence microscopy. NS4B was localized predominantly in the ER, which is consistent with previous reports[33] (Fig. 2A). Cardif was localized in mitochondria but did not colocalize with the ER-resident host protein disulphide-isomerase (PDI). Interestingly, Cardif and NS4B colocalized partly at the boundary of

the two proteins, although their original localization was different (Fig. 2A,C). STING was localized predominantly in the ER[20,21] (Fig. 2B,D). STING colocalized partly with Cardif, which is consistent with a previous report by Ishikawa and Barber[20] (Fig. 2B,D). In cells cotransfected with NS4B and STING expression plasmids, NS4B colocalized precisely with STING (Fig. 2B,D). To examine the region of NS4B-STING interaction, we next observed the two proteins by performing staining for them along with mitochondria-associated ER membrane (MAM), which is a physical association with mitochondria[34] and has been reported the site of Cardif-STING association.[24] Both NS4B and STING were adjacent to and partially colocalized
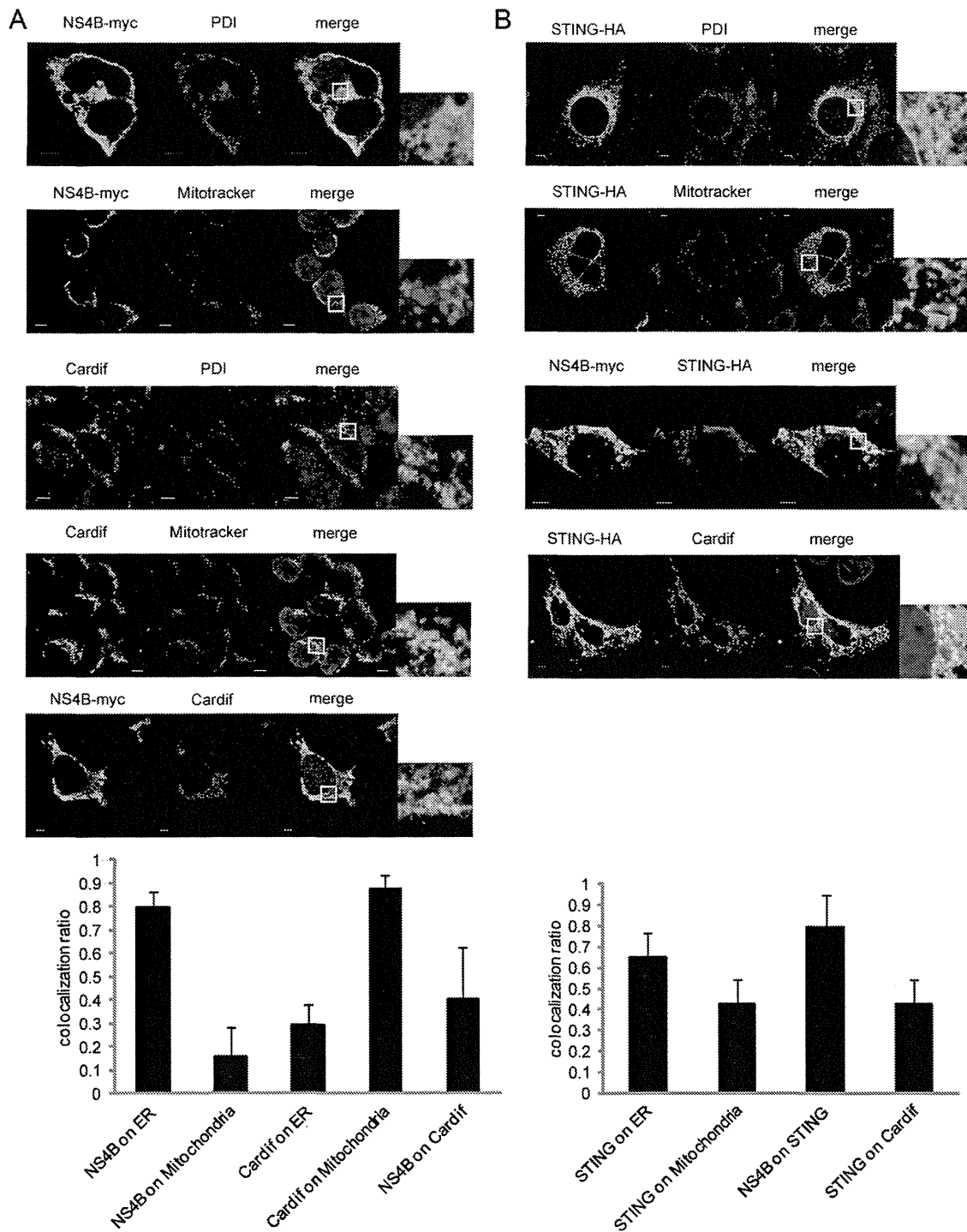
Fig. 2. Subcellular localization of NS4B, Cardif, and STING. (A-D) Subcellular localization of NS4B, Cardif, and STING in 293T (A,C) and Huh7 (B,D) cells. (A,C) NS4B-myc (first, second, and fifth panels of A and third panel of C) was transfected, and 24 hours later the cells were fixed and immunostained with anti-myc. In the third, fourth, and fifth panels of A, and the first and second panels of C, endogenous Cardif was detected with anti-Cardif antibody. ER was immunostained with anti-PDI antibody (first and third panels of A and first panel of C). Mitochondria were stained using Mitotracker (second and fourth panels of A and second panel of C). Nuclei were stained with 4',6-diamidino-2-phenylindole (DAPI). (B,D) STING-HA (all panels) and NS4B-myc (third panels) were transfected, and after 24 hours the cells were fixed and immunostained with anti-HA or anti-myc, respectively. In the fourth panels, endogenous Cardif was detected with anti-Cardif antibody. ER was immunostained with anti-PDI antibody (first panels). Mitochondria were stained using Mitotracker (second panels). Nuclei were stained with DAPI. (E) NS4B-myc and STING-HA were transfected into Huh7 cells and after 24 hours the cells were fixed and immunostained with anti-HA, anti-myc, and anti-FACL4 (MAM) antibody. Cells were visualized by confocal microscopy. Scale bars indicate 5 μm. In each microscopic image, the grade of protein colocalization in a single cell was quantified and is shown in the graphs at the bottom of each panel. Values are shown as the average colocalization ratio in 8 cells. Error bars indicate the mean + SD.

Fig. 2. Continued

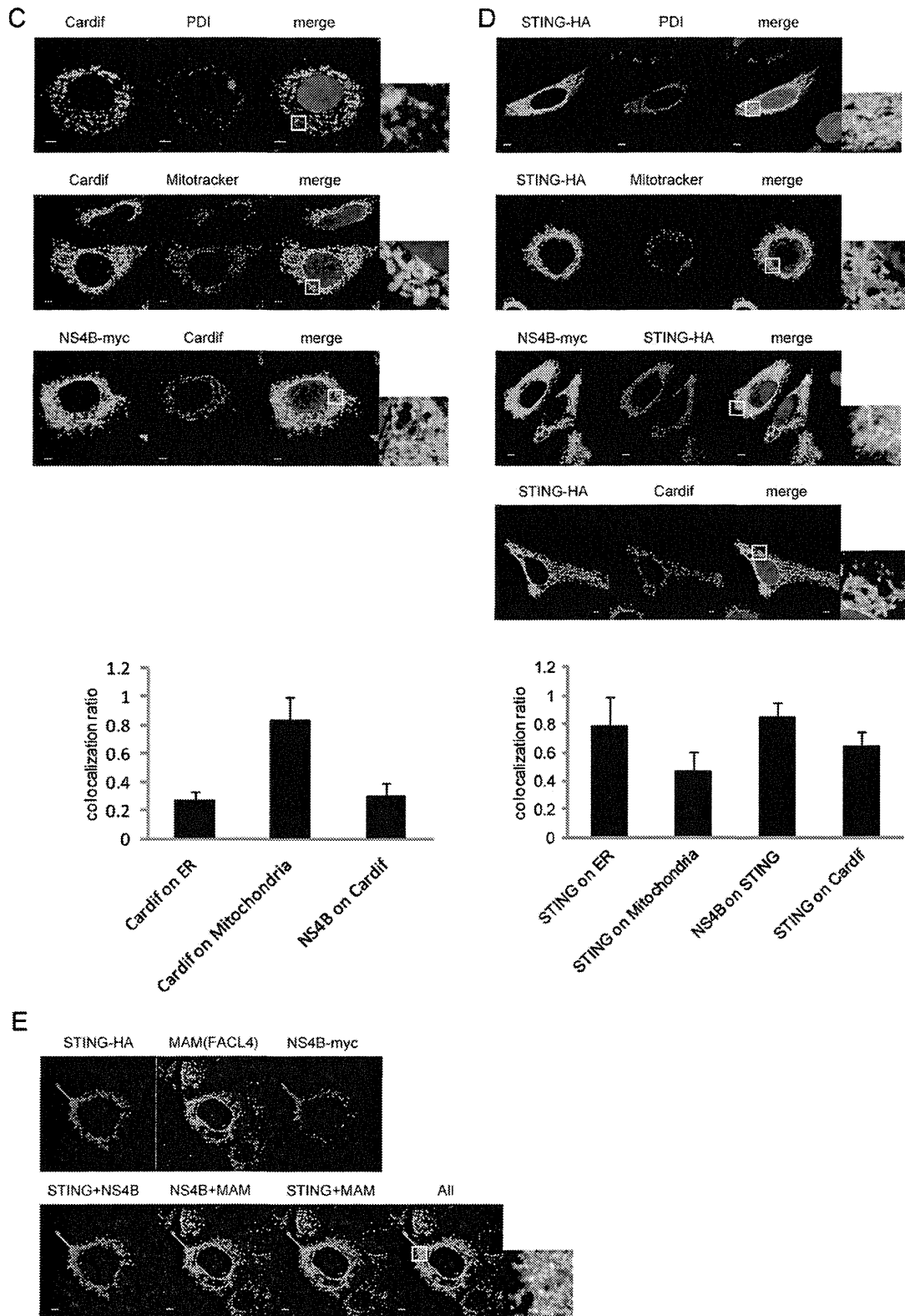with fatty acid-CoA ligase long chain 4 (FACL4), which is a MAM marker protein[35,36] (Fig. 2E). These findings suggest that NS4B might interact with STING on MAM more strongly than with Cardif.

***Protein-Protein Interaction Between NS4B, Cardif, and STING.*** Knowing that NS4B was colocalized strongly with STING and only partly with Cardif, we next analyzed direct protein-protein interactions
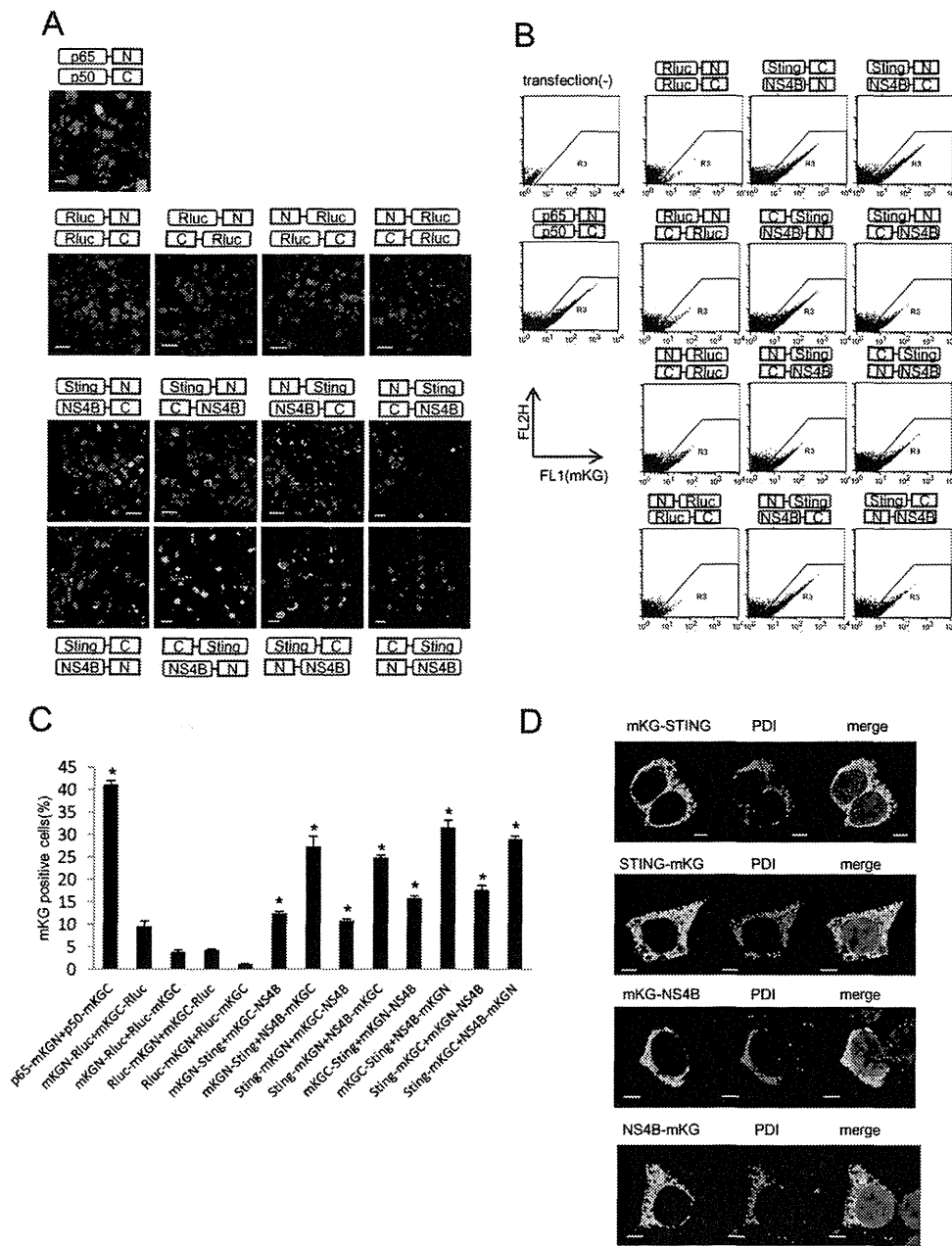
**A**



**B**



**C**



**D**



Fig. 3. BiFC assays of STING and NS4B. The complementary pairs of N- or C-terminally mKG-fused NS4B and STING expression plasmids were cotransfected in HEK293T cells. After 24 hours, the cells were fixed and observed by confocal microscopy (A) or subjected to flow cytometry to measure mKG-emitted fluorescence (BiFC signal) and to count BiFC signal-positive cells (B,C). Plasmids expressing p65-mKGN and p50-mKGC individually were used as a BiFC-positive control and plasmids expressing N- or C-terminally mKG fused Rluc were used as a negative control. The letters N and C denote complimentary N- and C-terminal fragments of mKG, respectively. Assays were performed in triplicate and error bars indicate the mean $\pm$ SD. Scale bars indicate 10 $\mu$m (A). *$P < 0.05$ compared with corresponding negative controls. (D) Plasmids expressing mKG fragment-fused STING or NS4B were transfected in HEK293T cells. After 24 hours, the cells were fixed and immunostained with anti-mKG and anti-PDI (ER) antibody. Nuclei were stained with DAPI. Cells were observed by confocal microscopy. Scale bars = 5 $\mu$m.

between NS4B, Cardif, and STING. To detect those interactions in living cells, we performed BiFC assays.[37,38] We constructed NS4B, Cardif, and STING expression plasmids that were N- or C-terminally fused with truncated mKG proteins, respectively. First, we cotransfected several different pairs of NS4B and STING expression plasmids that were fused with complementary pairs of N- or C-terminally truncated mKG. Strong fluorescence by mKG complexes (BiFC signal) was detected in all pairs of cotransfections, suggesting significant molecular interaction (Fig. 3A). In flow cytometry, all pairs of NS4B- and STING-mKG fusion proteins were positive for strong BiFC signal (Fig. 3B). The percentages of cells positive for BiFC

signal were significantly higher in STING-mKG and NS4B-mKG fusion complexes than in corresponding controls (Fig. 3C). These results demonstrate that HCV-NS4B and STING proteins interact with each other strongly and specifically in cells. Fluorescence microscopy indicated that N- and C-terminal fusion of mKG onto NS4B and STING did not affect subcellular localization (Fig. 3D).

We next studied the molecular interaction between NS4B and Cardif by BiFC assay using NS4B and Cardif fusion plasmids that were tagged with complementary pairs of truncated mKG. Weak fluorescence was detected in cells transfected with the pairs N-Cardif and NS4B-C, N-Cardif and C-NS4B, C-Cardif and
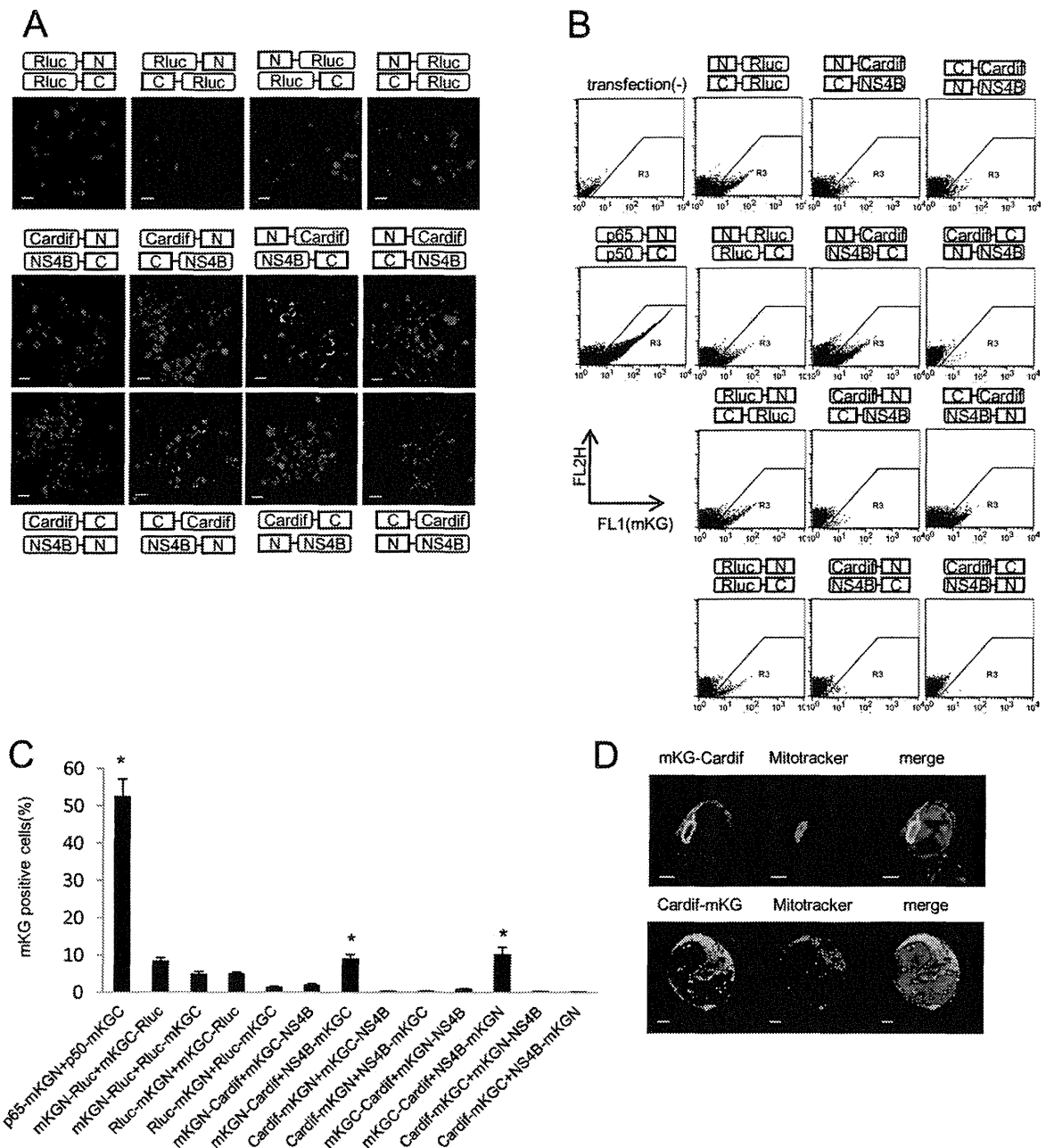
Fig. 4. BiFC assays of Cardif and NS4B. The complementary pairs of N- or C-terminally mKG-fused NS4B and Cardif expression plasmids were cotransfected in HEK293T cells. After 24 hours, the cells were fixed and observed by confocal microscopy (A) or subjected to flow cytometry to measure mKG-emitted fluorescence (BiFC signal) and to count BiFC signal-positive cells (B,C). Plasmids expressing p65-mKGN and p50-mKGC individually were used as a BiFC-positive control and plasmids expressing N- or C-terminally mKG-fused Rluc were used as a negative control. The letters N and C denote complimentary N- and C-terminal fragments of mKG, respectively. Assays were performed in triplicate, and error bars indicate the mean ± SD. Scale bars indicate 10 $\mu$m (A). *$P$ < 0.05 compared with corresponding negative controls. (D) Plasmids expressing mKG fragment-fused STING or NS4B were transfected in HEK293T cells. After 24 hours, the cells were fixed and immunostained with anti-mKG antibody. Mitochondria were stained using Mitotracker, and nuclei were stained with DAPI. Cells were observed by confocal microscopy. Scale bars = 5 $\mu$m.

NS4B-N, and C-Cardif and N-NS4B (Fig. 4A,B). The percentage of cells positive for BiFC signal increased with the combination of N-Cardif and NS4B-C, and C-Cardif and NS4B-N (Fig. 4C). Fluorescence microscopy indicated that mKG-Cardif, but not Cardif-mKG, was partially colocalized with mitochondria, possibly due to disruption of mitochondria anchor domain by C-terminal fusion with mKG (Fig. 4D). These results indicate the lack of significant molecular interactions between NS4B and Cardif.

**Binding of NS4B to STING Blocks Molecular Interaction Between Cardif and STING.** It has been reported that STING binds Cardif directly.[20,22] Thus, we hypothesized that NS4B, through a competitive
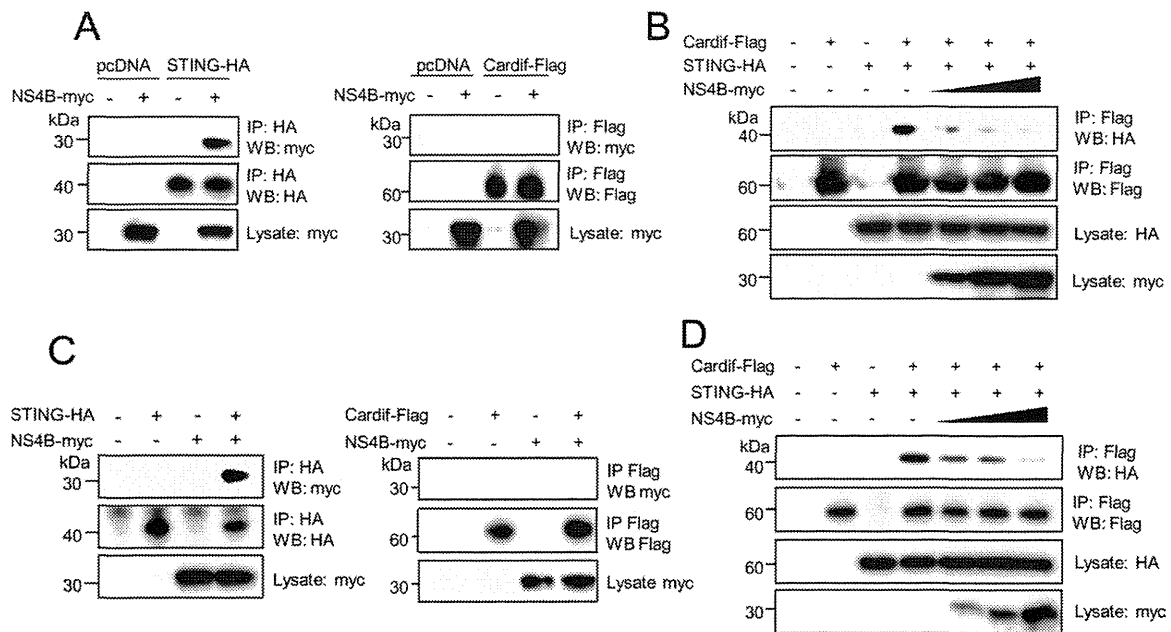
Fig. 5. Binding of NS4B to STING blocks molecular the interaction between Cardif and STING. (A,C) NS4B expression plasmid was cotransfected with STING or Cardif expression plasmid into HEK293T cells (A) or Huh7 cells (C). After 24 hours, cell lysates were subjected to immunoprecipitation using anti-HA or anti-Flag and were immunoblotted with anti-myc. (B,D) Cardif and STING expression plasmids were cotransfected with various amounts of NS4B plasmid in HEK293T cells (B) or Huh7 cells (D). After 24 hours, cells lysates were subjected to immunoprecipitation using anti-Flag and were immunoblotted with anti-HA.

interaction with STING, may hinder the direct molecular interaction between Cardif and STING. To verify this hypothesis, we performed immunoprecipitation assays. First, we transfected plasmids that expressed NS4B and Cardif, or NS4B and STING, in HEK293T cells or Huh7 cells, and performed immunoprecipitation. NS4B strongly bound to STING in both HEK293T cells and Huh7 cells, suggesting specific molecular interactions, whereas NS4B and Cardif did not show any obvious interaction (Fig. 5A,C). Consistent with previous reports, STING and Cardif showed significant interaction (Fig. 5B,D). Interestingly, those interactions were decreased by coexpression of NS4B, depending on its input amount, and finally blocked completely in both HEK293T and Huh7 cells (Fig. 5B,D). Collectively, the results above demonstrate that NS4B disrupts the interaction between Cardif and STING possibly through competitive binding to STING.

*Effects on HCV Infection and Replication Levels by STING Knockdown and NS4B Overexpression.* We next studied the impact of STING-mediated IFN production and its regulation by NS4B on HCV infection and cellular replication. First, we transfected three STING-targeted siRNAs into Huh7/Feo cells (Fig. 6A). As shown in Fig. 6B, STING knockdown cells conferred significantly higher permissibility to HCV replication. We next transfected HCV-JFH1 RNA into Huh7 cells that were transiently transfected with NS4B. As shown

in Fig. 6C, HCV core protein expression was significantly higher in NS4B-overexpressed cells. Furthermore, HCV replication was increased significantly in Huh7/Feo cells overexpressing NS4B (Fig. 6D). Taken together, the results above demonstrate that STING and NS4B may negatively or positively regulate cellular permissiveness to HCV replication.

*The N-terminal Domain of NS4B Is Essential for Suppressing IFN-β Promoter Activity Mediated by RIG-I, Cardif, and STING.* It has been reported that the N-terminal domain of several forms of flaviviral NS4B shows structural homology with STING.[24] We therefore investigated whether the STING homology domain in NS4B is responsible for suppression of IFN-β production. We constructed two truncated NS4B expression plasmids, which covered the N terminus (NS4Bt1-84, amino acids 1 through 84) containing the STING homology domain and the C terminus (NS4Bt85-261, amino acids 85 through 261), respectively (Fig. 7A). Immunoblotting showed that NS4Bt1-84 and NS4Bt85-261 yielded protein bands of ~9 kDa and ~20 kDa, respectively. Aberrant bands in the truncated NS4B may be due to alternative posttranslational processing. HEK293T cells were transfected with ΔRIG-I, Cardif, or STING, and NS3/4A or the truncated NS4B, along with IFN-β-Fluc plasmid, and a reporter assay was performed. NS4Bt1-84 significantly suppressed RIG-I, Cardif, and STING-
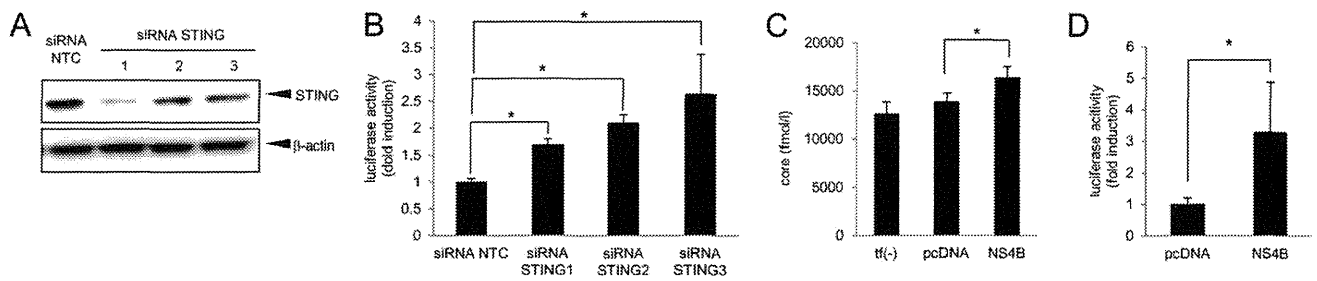
Fig. 6. Effects on HCV replication levels by STING knockdown and NS4B overexpression. (A) Effects of siRNA knockdown of STING by siRNA. Huh7 cells were transfected with STING-targeted siRNAs (siRNA STING-1, -2, and -3, respectively) or negative control siRNA (siRNA NTC). Seventy-two hours after transfection, cells were harvested and expression levels of STING protein were detected by immunoblotting. (B) Huh7 cells expressing HCV-Feo subgenomic replicon (Huh7/Feo)[27,28] were transfected with STING-targeted siRNAs or negative control siRNA. Seventy-two hours after transfection, cells were harvested, and internal luciferase activities were measured. The $y$ axis indicates luciferase activity shown as a ratio of transfection-negative control. Assays were performed in triplicate, and error bars indicate the mean + SD. *$P < 0.05$ compared with corresponding negative controls. (C) Empty plasmid or plasmid expressing NS4B was transfected into Huh7 cells. After 24 hours, HCV-JFH1 RNA was transfected into these cells. Seventy-two hours after virus transfection, HCV core antigen levels in culture medium were measured. Assays were performed in triplicate, and error bars indicate the mean + SD. *$P < 0.05$ compared with corresponding negative controls. tf($-$), transfection-negative control. (D) Huh7 cells expressing HCV-Feo replicon (Huh7/Feo)[27,28] were transfected with NS4B expressing plasmid or empty plasmid (pcDNA). Forty-eight hours after transfection, internal luciferase activities were measured. The $y$ axis indicates luciferase activity shown as a ratio of the transfection-negative control. Assays were performed in triplicate, and error bars indicate the mean + SD. *$P < 0.05$ compared with corresponding negative controls.

induced IFN-$\beta$ promoter activity, whereas NS4Bt85-261 did not (Fig. 7B). These results suggest that the N-terminal domain of NS4B is responsible for association with STING. Fluorescent microscopy indicated that both NS4Bt1-84 and NS4Bt85-26 colocalized with ER and STING (Fig. 7C).

**NS4B Suppresses IFN Production Signaling Cooperatively with NS3/4A.** It has been reported that
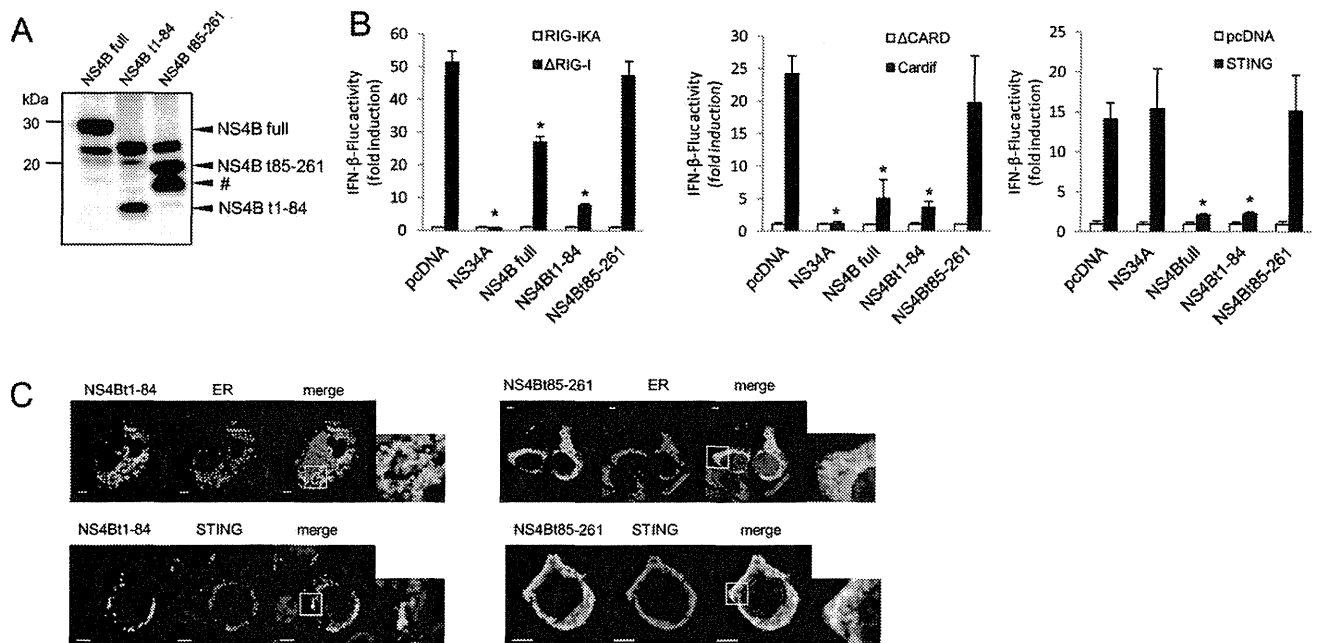


Fig. 7. The N-terminal domain of NS4B is essential for suppressing IFN-$\beta$ promoter activity induced by RIG-I, Cardif, or STING. (A) Immunoblotting of NS4B and truncated NS4B, NS4B t1-84, and NS4Bt85-216. HEK293T cells were transfected with NS4B or truncated NS4B. After 24 hours, the cells were lysed and immunoblot assays were performed. The band indicated by the pound sign (#) is a truncated NS4B, probably generated via alternative posttranslational processing. (B) Plasmids expressing ΔRIG-I, Cardif, or STING as well as NS3/4A or the indicated truncated form of NS4B were cotransfected with pIFN-$\beta$-Fluc and pRL-CMV in HEK293T cells. Dual luciferase assays were performed 24 hours after transfection. Plasmids expressing RIG-IKA, ΔCARD, or pcDNA were used as negative controls. The $y$ axis indicates IFN-$\beta$-Fluc activity shown as relative values. Assays were performed in triplicate, and error bars indicate the mean ± SD. *$P < 0.05$ compared with corresponding negative controls. (C) Plasmids expressing NS4Bt1-84-myc of NS4Bt85-261-myc were transfected with or without plasmids expressing HA-STING in HEK293T cells. After 24 hours, the cells were fixed and immunostained. Nuclei were stained with DAPI. Cells were observed by confocal microscopy. Scale bars indicate 5 μm.
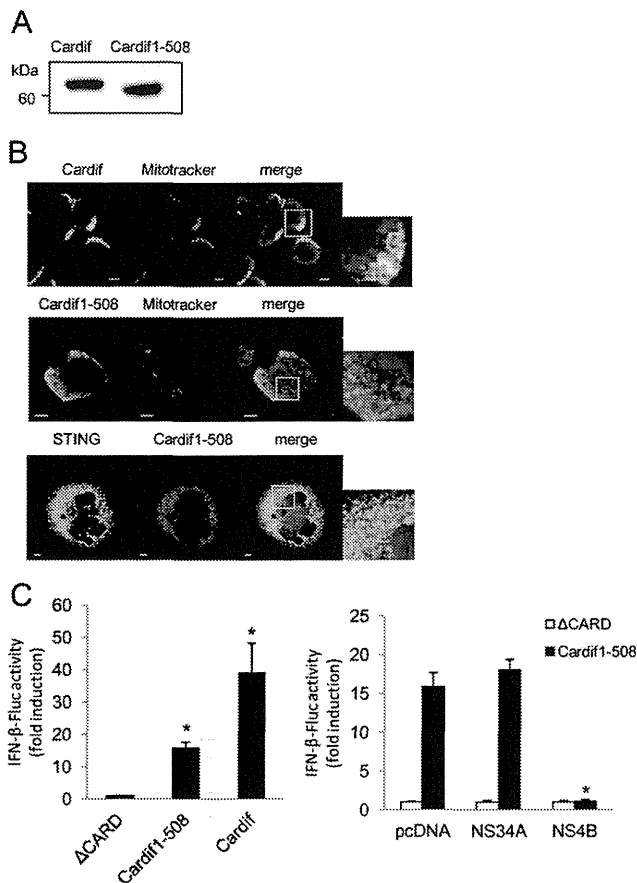
## A

Cardif   Cardif1-508



## B

Cardif      Mitotracker      merge



Cardif1-508   Mitotracker      merge



STING       Cardif1-508      merge



## C



Fig. 8. NS4B suppressed IFN-$\beta$ production pathway independently of and cooperatively with NS3/4A. (A) Immunoblotting of Cardif and truncated Cardif (Cardif1-508). HEK293T cells were transfected with Cardif or truncated Cardif (Cardif1-508). After 24 hours, the cells were lysed and immunoblot assays were performed. (B) Subcellular localization of Cardif and truncated Cardif (Cardif1-508). HEK293T cells were immunostained with anti-Cardif antibody or HEK293T cells were transfected with myc-tagged truncated Cardif (Cardif1-508-myc), and after 24 hours the cells were immunostained with anti-myc. Mitochondria were stained with Mitotracker (red) and nuclei were stained with DAPI (blue). Plasmid expressing myc-tagged truncated Cardif (Cardif1-508) and plasmid expressing HA-tagged STING were transfected into HEK293T cells. The cells were immunostained with anti-myc and anti-HA antibodies and analyzed by confocal laser microscopy. Scale bars = 10 $\mu$m. (C) Plasmids expressing Cardif or truncated Cardif (Cardif1-508) and pIFN-$\beta$-Fluc and pRL-CMV were transfected with or without plasmid expressing NS3/4A or NS4B into HEK293T cells as indicated. Dual luciferase assays were performed 24 hours after transfection. Plasmid expressing $\Delta$CARD or pcDNA was used as a negative control. The $y$ axis indicates IFN-$\beta$-Fluc activity shown as relative values. Assays were performed in triplicate, and error bars indicate the mean $\pm$ SD. *$P < 0.05$.

HCV NS3/4A serine protease cleaves Cardif between Cys-508 and His-509, releases Cardif from the mitochondrial membrane, and blocks RIG-I–induced IFN-$\beta$ production. We next assessed whether NS4B suppresses IFN-$\beta$ production in the presence of Cardif cleaved by NS3/4A protease (Cardif1-508, Fig. 8A). The truncation of Cardif–C-terminal residue abolished mitochondrial localization but still colocalized with

STING (Fig. 8B). The reporter assay showed that Cardif1-508 induced weak IFN-$\beta$ activation. Interestingly, NS4B completely blocked the residual function of the Cardif1-508 protein to activate IFN-$\beta$ expression, suggesting an additive effect of NS3/4A and NS4B on the RIG-I–activating pathway (Fig. 8C).

## Discussion

It has been reported that viruses, including HCV, target IFN signaling to establish persistent replication in host cells.[39] We have reported that NS4B blocks the transcriptional activation of ISRE induced by overexpression of RIG-I and Cardif, but not by TBK1 or IKK$\epsilon$.[19] In the present study, we have shown that NS4B directly and specifically binds STING, an ER-residing scaffolding protein of Cardif and TBK1 and an inducer of IFN-$\beta$ production (Figs. 3 and 5), and blocked the interaction between STING and Cardif (Fig. 5B,D) resulting in strong suppression of RIG-I–mediated phosphorylation of IRF-3 and expressional induction of IFN-$\beta$ (Fig. 1). Furthermore, HCV replication was increased by knockdown of STING or overexpression of NS4B (Fig. 6). Taken together, our results demonstrate that HCV-NS4B strongly blocks virus-induced, RIG-I–mediated activation of IFN-$\beta$ production signaling through targeting STING, which constitutes a novel mechanism of viral evasion from innate immune responses and establishment of persistent viral replication.

Our results also showed that the effects of NS4B on the RIG-I signaling were independent of NS3/4A-mediated cleavage of Cardif. Reporter assays showed that a cleaved form of Cardif (Cardif1-508) partially retained activity for the induction of IFN-$\beta$ promoter activation. The residual IFN-$\beta$ promoter activation was suppressed almost completely by NS4B but not by NS3/4A (Fig. 8C). These findings show that there are at least two mechanisms by which HCV can abrogate RIG-I–mediated IFN production signaling to accomplish abrogation of cellular antiviral responses.

NS4B and STING are ER proteins,[20,21,40] whereas Cardif is localized on the outer mitochondrial membrane.[9] Consistent with those reports, our immunostaining experiments demonstrated that most NS4B protein colocalized with STING (Fig. 2), and their association was localized on MAM (Fig. 2E). In addition to the significant colocalization of STING and NS4B, STING partially colocalized with Cardif at the boundary region of the two proteins (Fig. 2B). Furthermore, immunoprecipitation experiments showed that overexpression of NS4B completely blocked the interaction of STING with Cardif (Fig. 5B). Ishikawa et al.[24] reported

that STING could associate with Cardif by MAM interaction. Castanier et al.[41] reported that Cardif-STING interaction was enhanced in cells with elongated mitochondria. In addition, Horner et al.[42,43] observed NS3/4A targeting of MAM-anchored synapse and cleavage of Cardif at MAM but not in mitochondria. These results led us to speculate that interaction between STING and Cardif was enhanced by altering their subcellular localization during viral infection and that NS4B inhibits Cardif activation by interfering with the association between STING and Cardif on MAM-like NS3/4A behavior against host innate immunity.

HCV-NS4B is an ER-localized 27-kDa protein with several functions in the HCV life cycle. Cellular expression of NS4B induces convolution of the ER membrane and formation of a membranous web that harbors HCV replicase complex.[44,45] NS4B also has RNA-binding capacity.[46] In addition, several point mutations of NS4B were found to alter viral replication activity.[33,46,47] The studies above indicate that NS4B provides an important protein-protein or protein-RNA interaction platform within the HCV replication complex and is essential for viral RNA replication. However, there are few reports on the involvement of NS4B with antiviral immune responses. Consistent with our previous study, Moriyama et al.[48] reported that NS4B partially inhibited dsRNA-induced but not TRIF-induced activation of IFN-β. In NS4B-expressing cells, IFN-α induced activation of STAT1 was suppressed.[49] The present study has demonstrated that NS4B functions against the host IFN response, such that NS4B directly interacts with STING and suppresses downstream signaling, resulting in the induction of IFN production.

STING contains a domain homologous to the N terminus of NS4B derived from several flaviviruses, including HCV. In our previous NS4B truncation assay, the NS4B N-terminal domain (amino acids 1-110) was important for suppression of RIG-I–induced IFN-β expression.[19] Consistent with these results, N-terminally truncated NS4B (NS4Bt1-84) significantly suppressed STING and Cardif-induced IFN-β promoter activation, whereas the C terminus of NS4B (NS4Bt85-261) did not (Fig. 7). These results reinforce our hypothesis that NS4B binds STING at its homology domain and blocks the ability of STING to induce IFN-β production.

A small molecule inhibitor of NS4B has been developed and is under preliminary clinical trials.[50] Einav et al.[51] identified clemizole hydrochloride, an H1 histamine receptor antagonist, as an inhibitor of the RNA-binding function of NS4B and HCV RNA replication. A phase 1B clinical trial of clemizole in hepatitis C patients has been completed.[52] Other two NS4B inhibitors which are a compound of amiloride analog and anguizole are under preclinical development.[53,54] The possibility remains that such NS4B inhibitors may suppress HCV replication partly through inhibiting the ability of NS4B to suppress IFN-β production and restore cellular antiviral responses.

In conclusion, IFN production signaling induced by HCV infection and mediated by RIG-I is suppressed by NS4B through a direct interaction with STING. These virus-host interactions help to elucidate the mechanisms of persistent HCV infection and constitute a potential target to block HCV infection.

# References

1. Samuel CE. Antiviral actions of interferons. Clin Microbiol Rev 2001; 14:778-809.
2. Taniguchi T, Takaoka A. The interferon-alpha/beta system in antiviral responses: a multimodal machinery of gene regulation by the IRF family of transcription factors. Curr Opin Immunol 2002;14:111-116.
3. Sakamoto N, Watanabe M. New therapeutic approaches to hepatitis C virus. J Gastroenterol 2009;44:643-649.
4. Bigger CB, Brasky KM, Lanford RE. DNA microarray analysis of chimpanzee liver during acute resolving hepatitis C virus infection. J Virol 2001;75:7059-7066.
5. Yoneyama M, Kikuchi M, Natsukawa T, Shinobu N, Imaizumi T, Miyagishi M, et al. The RNA helicase RIG-I has an essential function in duoble-stranded RNA-induced innate antiviral responses. Nat Immunol 2004;5:730-737.
6. Hornung V, Ellegast J, Kim S, Brzozka K, Jung A, Kato H, et al. 5'-Triphosphate RNA is the ligand for RIG-I. Science 2006;314:994-997.
7. Takahasi K, Yoneyama M, Nishihori T, Hirai R, Kumeta H, Narita R, et al. Nonself RNA-sensing mechanism of RIG-I helicase and activation of antiviral immune responses. Mol Cell 2008;29:428-440.
8. Kawai T. IPS-1, an adaptor triggering RIG-I- and Mda5-mediated type I interferon induction. Nat Immunol 2005;6:981-988.
9. Seth RB, Sun L, Ea CK, Chen ZJ. Identification and characterization of MAVS, a mitochondrial antiviral signaling protein that activates NF-κB and IRF 3. Cell 2005;122:669-682.
10. Xu LG. VISA is an adapter protein required for virus-triggered IFN-β signaling. Mol Cell 2005;19:727-740.
11. Meylan E, Curran J, Hofmann K, Moradpour D, Binder M, Bartenschlager R, et al. Cardif is an adaptor protein in the RIG-I antiviral pathway and is targeted by hepatitis C virus. Nature 2005;437: 1167-1172.
12. Yoneyama M, Suhara W, Fukuhara Y, Fukuda M, Nishida E, Fujita T. Direct triggering of the type I interferon system by virus infection: activation of a transcription factor complex containing IRF-3 and CBP/p300. EMBO J 1998;17:1087-1095.

13. Lin W, Kim SS, Yeung E, Kamegaya Y, Blackard JT, Kim KA, et al. Hepatitis C virus core protein blocks interferon signaling by interaction with the STAT1 SH2 domain. J Virol 2006;80:9226-9235.

14. Suda G, Sakamoto N, Itsui Y, Nakagawa M, Tasaka-Fujita M, Funaoka Y, et al. IL-6-mediated intersubgenotypic variation of interferon sensitivity in hepatitis C virus genotype 2a/2b chimeric clones. Virology 2010;407:80-90.

15. Funaoka Y, Sakamoto N, Suda G, Itsui Y, Nakagawa M, Kakinuma S, et al. Analysis of interferon signaling by infectious hepatitis C virus clones with substitutions of core amino acids 70 and 91. J Virol 2011; 85:5986-5994.

16. Loo YM, Owen DM, Li K, Erickson AK, Johnson CL, Fish PM, et al. Viral and therapeutic control of IFN-beta promoter stimulator 1 during hepatitis C virus infection. Proc Natl Acad Sci U S A 2006;103:6001-6006.

17. Li X-D, Sun L, Seth RB, Pineda G, Chen ZJ. Hepatitis C virus protease NS3/4A cleaves mitochondrial antiviral signaling protein off the mitochondria to evade innate immunity. Proc Natl Acad Sci U S A 2005; 102:17717-17722.

18. Baril M, Racine M-E, Penin F, Lamarre D. MAVS Dimer Is a Crucial Signaling Component of Innate Immunity and the Target of Hepatitis C Virus NS3/4A Protease. J. Virol. 2009;83:1299-1311.

19. Tasaka M, Sakamoto N, Itakura Y, Nakagawa M, Itsui Y, Sekine-Osajima Y, et al. Hepatitis C virus non-structural proteins responsible for suppression of the RIG-I/Cardif-induced interferon response. J Gen Virol 2007;88:3323-3333.

20. Ishikawa H, Barber GN. STING is an endoplasmic reticulum adaptor that facilitates innate immune signalling. Nature 2008;455:674-678.

21. Sun W, Li Y, Chen L, Chen H, You F, Zhou X, et al. ERIS, an endoplasmic reticulum IFN stimulator, activates innate immune signaling through dimerization. Proc Natl Acad Sci U S A 2009;106:8653-8658.

22. Zhong B, Yang Y, Li S, Wang YY, Li Y, Diao F, et al. The adaptor protein MITA links virus-sensing receptors to IRF3 transcription factor activation. Immunity 2008;29:538-550.

23. Jin L. MPYS, a novel membrane tetraspanner, is associated with major histocompatibility complex class II and mediates transduction of apoptotic signals. Mol Cell Biol 2008;28:5014-5026.

24. Ishikawa H, Ma Z, Barber GN. STING regulates intracellular DNA-mediated, type I interferon-dependent innate immunity. Nature 2009; 461:788-792.

25. Yanagi M, Purcell RH, Emerson SU, Bukh J. Transcripts from a single full-length cDNA clone of hepatitis C virus are infectious when directly trasfected into the liver of a chimpanzee. Proc Natl Acad Sci U S A 1997;94:8738-8743.

26. Lin R, Lacoste J, Nakhaei P, Sun Q, Yang L, Paz S, et al. Dissociation of a MAVS/IPS-1/VISA/Cardif-IKKepsilon molecular complex from the mitochondrial outer membrane by hepatitis C virus NS3-4A proteolytic cleavage. J Virol 2006;80:6072-6083.

27. Yokota T, Sakamoto N, Enomoto N, Tanabe Y, Miyagishi M, Maekawa S, et al. Inhibition of intracellular hepatitis C virus replication by synthetic and vector-derived small interfering RNAs. EMBO Rep 2003;4:602-608.

28. Tanabe Y, Sakamoto N, Enomoto N, Kurosaki M, Ueda E, Maekawa S, et al. Synergistic inhibition of intracellular hepatitis C virus replication by combination of ribavirin and interferon- alpha. J Infect Dis 2004;189:1129-1139.

29. Wakita T, Pietschmann T, Kato T, Date T, Miyamoto M, Zhao Z, et al. Production of infectious hepatitis C virus in tissue culture from a cloned viral genome. Nat Med 2005;11:791-796.

30. Lindenbach BD, Evans MJ, Syder AJ, Wolk B, Tellinghuisen TL, Liu CC, et al. Complete replication of hepatitis C virus in cell culture. Science 2005;309:623-626.

31. Nakagawa M, Sakamoto N, Enomoto N, Tanabe Y, Kanazawa N, Koyama T, et al. Specific inhibition of hepatitis C virus replication by cyclosporin A. Biochem Biophys Res Commun 2004;313:42-47.

32. Yamashiro T, Sakamoto N, Kurosaki M, Kanazawa N, Tanabe Y, Nakagawa M, et al. Negative regulation of intracellular hepatitis C virus replication by interferon regulatory factor 3. J Gastroenterol 2006;41:750-757.

33. Lindstrom H, Lundin M, Haggstrom S, Persson MA. Mutations of the hepatitis C virus protein NS4B on either side of the ER membrane

34. Hayashi T, Rizzuto R, Hajnoczky G, Su TP. MAM: more than just a housekeeper. Trends Cell Biol 2009;19:81-88.

35. Lewin TM, Van Horn CG, Krisans SK, Coleman RA. Rat liver acyl-CoA synthetase 4 is a peripheral-membrane protein located in two distinct subcellular organelles, peroxisomes, and mitochondrial-associated membrane. Arch Biochem Biophys 2002;404:263-270.

36. Simmen T, Aslan JE, Blagoveshchenskaya AD, Thomas L, Wan L, Xiang Y, et al. PACS-2 controls endoplasmic reticulum-mitochondria communication and Bid-mediated apoptosis. EMBO J 2005;24:717-729.

37. Kerppola TK. Design and implementation of bimolecular fluorescence complementation (BiFC) assays for the visualization of protein interactions in living cells. Nat Protoc 2006;1:1278-1286.

38. Kerppola TK. Bimolecular fluorescence complementation (BiFC) analysis as a probe of protein interactions in living cells. Annu Rev Biophys 2008;37:465-487.

39. Kato H. Differential roles of MDA5 and RIG-I helicases in the recognition of RNA viruses. Nature 2006;441:101-105.

40. Saitoh T, Fujita N, Hayashi T, Takahara K, Satoh T, Lee H, et al. Atg9a controls dsDNA-driven dynamic translocation of STING and the innate immune response. Proc Natl Acad Sci U S A 2009;106: 20842-20846.

41. Castanier C, Garcin D, Vazquez A, Arnoult D. Mitochondrial dynamics regulate the RIG-I-like receptor antiviral pathway. EMBO Rep 2009;11:133-138.

42. Horner SM, Liu HM, Park HS, Briley J, Gale M. Mitochondrial-associated endoplasmic reticulum membranes (MAM) form innate immune synapses and are targeted by hepatitis C virus. Proc Natl Acad Sci U S A 2011;108:14590-14595.

43. Horner SM, Park HS, Gale M Jr. Control of innate immune signaling and membrane targeting by the hepatitis C virus NS3/4A protease are governed by the NS3 helix $\alpha$0. J Virol 2012;86:3112-3120.

44. Egger D, Wolk B, Gosert R, Bianchi L, Blum HE, Moradpour D, et al. Expression of Hepatitis C virus proteins induces distinct membrane alterations including a candidate viral replication complex. J Virol 2002;76:5974-5984.

45. Gretton SN, Taylor AI, McLauchlan J. Mobility of the hepatitis C virus NS4B protein on the endoplasmic reticulum membrane and membrane-associated foci. J Gen Virol 2005;86:1415-1421.

46. Einav S, Elazar M, Danieli T, Glenn JS. A nucleotide binding motif in hepatitis C virus (HCV) NS4B mediates HCV RNA replication. J Virol 2004;78:11288-11295.

47. Elazar M, Liu P, Rice CM, Glenn JS. An N-terminal amphipathic helix in hepatitis C virus (HCV) NS4B mediates membrane association, correct localization of replication complex proteins, and HCV RNA replication. J Virol 2004;78:11393-11400.

48. Moriyama M, Kato N, Otsuka M, Shao RX, Taniguchi H, Kawabe T, et al. Interferon-beta is activated by hepatitis C virus NS5B and inhibited by NS4A, NS4B, and NS5A. Hepatol Int 2007;1:302-310.

49. Xu J, Liu S, Xu Y, Tien P, Gao G. Identification of the nonstructural protein 4B of hepatitis C virus as a factor that inhibits the antiviral activity of interferon-alpha. Virus Res 2009;141:55-62.

50. Hofmann WP, Zeuzem S. A new standard of care for the treatment of chronic HCV infection. Nat Rev Gastroenterol Hepatol 2011;8: 257-264.

51. Einav S, Gerber D, Bryson PD, Sklan EH, Elazar M, Maerkl SJ, et al. Discovery of a hepatitis C target and its pharmacological inhibitors by microfluidic affinity analysis. Nat Biotech 2008;26:1019-1027.

52. Rai R, Deval J. New opportunities in anti-hepatitis C virus drug discovery: targeting NS4B. Antiviral Res 2011;90:93-101.

53. Cho NJ, Dvory-Sobol H, Lee C, Cho SJ, Bryson P, Masek M, et al. Identification of a class of HCV inhibitors directed against the nonstructural protein NS4B. Sci Transl Med 2010;2:15ra16.

54. Bryson PD, Cho NJ, Einav S, Lee C, Tai V, Bechtel J, et al. A small molecule inhibits HCV replication and alters NS4B's subcellular distribution. Antiviral Res 2010;87:1-8.

affect the efficiency of subgenomic replicons. Virus Res 2006;121: 169-178.

# Discrete Nature of EpCAM$^+$ and CD90$^+$ Cancer Stem Cells in Human Hepatocellular Carcinoma

Taro Yamashita,[1] Masao Honda,[1] Yasunari Nakamoto,[1] Masayo Baba,[1] Kouki Nio,[1] Yasumasa Hara,[1] Sha Sha Zeng,[1] Takehiro Hayashi,[1] Mitsumasa Kondo,[1] Hajime Takatori,[1] Tatsuya Yamashita,[1] Eishiro Mizukoshi,[1] Hiroko Ikeda,[1] Yoh Zen,[1] Hiroyuki Takamura,[1] Xin Wei Wang,[2] and Shuichi Kaneko[1]

Recent evidence suggests that hepatocellular carcinoma (HCC) is organized by a subset of cells with stem cell features (cancer stem cells; CSCs). CSCs are considered a pivotal target for the eradication of cancer, and liver CSCs have been identified by the use of various stem cell markers. However, little information is known about the expression patterns and characteristics of marker-positive CSCs, hampering the development of personalized CSC-targeted therapy. Here, we show that CSC markers EpCAM and CD90 are independently expressed in liver cancer. In primary HCC, EpCAM$^+$ and CD90$^+$ cells resided distinctively, and gene-expression analysis of sorted cells suggested that EpCAM$^+$ cells had features of epithelial cells, whereas CD90$^+$ cells had those of vascular endothelial cells. Clinicopathological analysis indicated that the presence of EpCAM$^+$ cells was associated with poorly differentiated morphology and high serum alpha-fetoprotein (AFP), whereas the presence of CD90$^+$ cells was associated with a high incidence of distant organ metastasis. Serial xenotransplantation of EpCAM$^+$/CD90$^+$ cells from primary HCCs in immune-deficient mice revealed rapid growth of EpCAM$^+$ cells in the subcutaneous lesion and a highly metastatic capacity of CD90$^+$ cells in the lung. In cell lines, CD90$^+$ cells showed abundant expression of c-Kit and *in vitro* chemosensitivity to imatinib mesylate. Furthermore, CD90$^+$ cells enhanced the motility of EpCAM$^+$ cells when cocultured *in vitro* through the activation of transforming growth factor beta (TGF-$\beta$) signaling, whereas imatinib mesylate suppressed *TGFB1* expression in CD90$^+$ cells as well as CD90$^+$ cell-induced motility of EpCAM$^+$ cells. *Conclusion:* Our data suggest the discrete nature and potential interaction of EpCAM$^+$ and CD90$^+$ CSCs with specific gene-expression patterns and chemosensitivity to molecular targeted therapy. The presence of distinct CSCs may determine the clinical outcome of HCC. (HEPATOLOGY 2012;00:000–000)

The cancer stem cell (CSC) hypothesis, which suggests that a subset of cells bearing stem-cell–like features is indispensable for tumor development, has recently been put forward subsequent to advances in molecular and stem cell biology. Liver cancer, including hepatocellular carci- noma (HCC), is a leading cause of cancer death worldwide.[1] Recent studies have shown the existence of CSCs in liver cancer cell lines and primary HCC specimens using various stem cell markers.[2-7] Inde- pendently, we have identified novel HCC subtypes defined by the hepatic stem/progenitor cell markers,

1

epithelial cell adhesion molecule (EpCAM) and alpha-fetoprotein (AFP), which correlate with distinct gene-expression signatures and prognosis.[8,9] EpCAM$^+$ HCC cells isolated from primary HCC and cell lines show CSC features, including tumorigenicity, invasiveness, and resistance to fluorouracil (5-FU).[10] Similarly, other groups have shown that CD133$^+$, CD90$^+$, and CD13$^+$ HCC cells are also CSCs, and that EpCAM, CD90, and CD133 are the only markers confirmed to enrich CSCs from primary HCCs thus far.[3-5,10]

Although EpCAM$^+$, CD90$^+$, and CD133$^+$ cells show CSC features, such as high tumorigenicity, an invasive nature, and resistance to chemo- and radiation therapy, it remains unclear whether these cells represent an identical HCC population and whether they share similar or distinct characteristics. In this study, we used fluorescent-activated cell sorting (FACS), microarray, and immunohistochemistry (IHC) techniques to investigate the expression patterns of the representative liver CSC markers CD133, CD90, and EpCAM in a total of 340 HCC cases and 7 cases of mesenchymal liver tumors. We further explored gene- and protein-expression patterns as well as tumorigenic capacity of sorted cells isolated from 15 primary HCCs and 7 liver cancer cell lines in an attempt to identify the molecular portraits of each cell type.

## Materials and Methods

*Clinical Specimens.* HCC samples were obtained with informed consent from patients who had undergone radical resection at the Liver Center in Kanazawa University Hospital (Kanazawa, Japan), and tissue acquisition procedures were approved by the ethics committee of Kanazawa University. A total of 102 formalin-fixed and paraffin-embedded HCC samples, obtained from 2001 to 2007, were used for IHC analyses. Fifteen fresh HCC samples were obtained between 2008 and 2012 from surgically resected specimens and an autopsy specimen and were used immediately to prepare single-cell suspensions and xenotransplantation (Table 1). Seven hepatic stromal tumors (three cavernous hemangioma, two hemangioendothelioma, and two angiomyolipoma) were formalin fixed and paraffin embedded and used for IHC analyses.

**Table 1. Clinicopathological Characteristics of HCC Cases Used for Xenotransplantation**

| ID | Age/Sex | Etiology | Tumor Size (cm) | Histological Grade | AFP (ng/mL) | DCP (IU/mL) |
|---|---|---|---|---|---|---|
| P1 | 77/M | Alcohol | 12.0 | Moderate | 198 | 322 |
| P2 | 61/F | NBNC | 11.0 | Moderate | 12 | 3,291 |
| P3 | 66/M | NBNC | 2.2 | Moderate | 13 | 45 |
| P4 | 65/M | HCV | 4.2 | Poor | 13,700 | 25,977 |
| P5 | 52/M | HBV | 6.0 | Moderate | 29,830 | 1,177 |
| P6 | 60/M | HCV | 2.7 | Poor | 249 | 185 |
| P7 | 79/F | HBV | 4.0 | Poor | 46,410 | 384 |
| P8 | 77/F | NBNC | 5.5 | Moderate | 17,590 | 562 |
| P9 | 71/M | Alcohol | 7.0 | Poor | 3,814 | 607 |
| P10 | 51/M | HBV | 2.2 | Well | <10 | 21 |
| P11 | 71/M | Alcohol | 2.1 | Well | <10 | 11 |
| P12 | 60/M | HBV | 10.8 | Poor | 323 | 2,359 |
| P13 | 66/M | HCV | 2.8 | Moderate | 11 | 29 |
| P14 | 71/M | HCV | 7.2 | Moderate | 235,700 | 375,080 |
| P15 | 75/M | HBV | 5.5 | Poor | <10 | 97 |

Abbreviation: DCP, des-gamma-carboxy prothrombin.

Additional details of experimental procedures are available in the Supporting Information.

## Results

*EpCAM, CD133, and CD90 Expression in HCC.* We first evaluated the frequencies of three representative CSC markers (EpCAM$^+$, CD90$^+$, and CD133$^+$ cells) in 12 fresh primary HCC cases surgically resected by FACS (representative data shown in Fig. 1A). Clinicopathological characteristics of primary HCC cases are shown in Table 1. We noted that frequency of EpCAM$^+$, CD90$^+$, and CD133$^+$ cells varied between individuals. Abundant CD90$^+$ (7.0%), but almost no EpCAM$^+$, cells (0.06%, comparable to the isotype control) were detected in P2, whereas few CD90$^+$ (0.6%), but abundant EpCAM$^+$, cells (17.5%) were detected in P4. Very small populations of EpCAM$^+$ (0.09%), CD90$^+$ (0.04%), and CD133$^+$ cells (0.05%) were found in P12, but they were almost nonexistent in P8, except for CD90$^+$ cells (0.08%) (Fig. 1A). We further evaluated the expression of EpCAM, CD90, and CD133 in xenografts obtained from surgically resected samples (P13 and P15) and an autopsy sample (P14). As a whole, compared to the isotype control, 7 of 15 HCCs contained definite EpCAM$^+$ cells (46.7%), whereas only 3 HCCs

Additional Supporting Information may be found in the online version of this article.
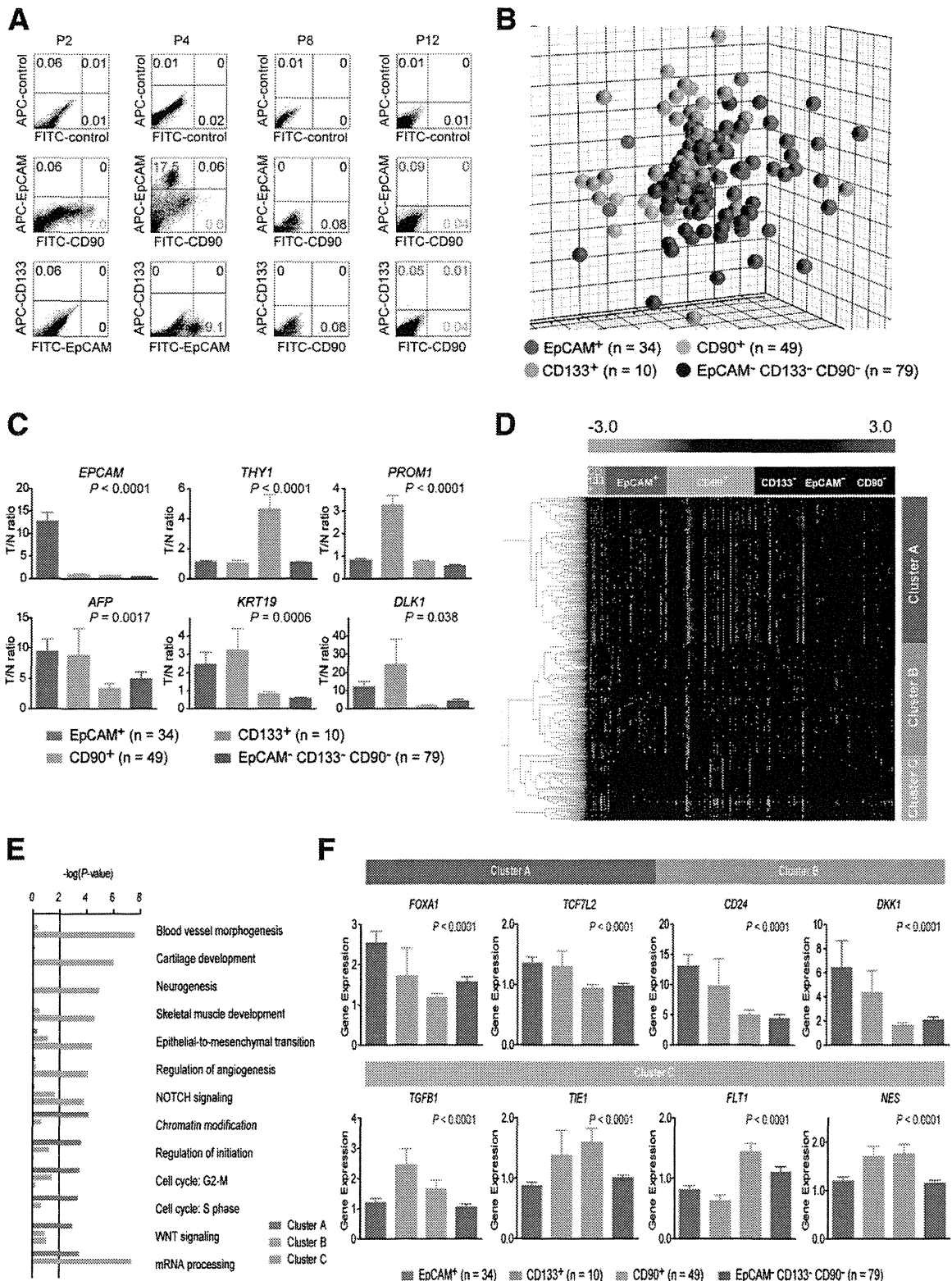
Fig. 1. Gene-expression profiles of CSC marker-positive HCCs. (A) FACS analysis of primary HCCs stained with fluorescent-labeled Abs against EpCAM, CD90, or CD133. (B) Multidimensional scaling analysis of 172 HCC cases characterized by the expression patterns of EpCAM, CD133, and CD90. Red, EpCAM$^+$ CD90$^-$ CD133$^-$ (n = 34); orange, EpCAM$^-$ CD90$^-$ CD133$^+$ (n = 10); light blue, EpCAM$^-$ CD90$^+$ CD133$^-$ (n = 49); blue, EpCAM$^-$ CD90$^-$ CD133$^-$ (n = 79). HCC specimens were clustered in specific groups with statistical significance ($P$ < 0.001). (C) Expression patterns of well-known hepatic stem/progenitor markers in each HCC subtype, as analyzed by microarray. Red bar, EpCAM$^+$; orange bar, CD133$^+$; light blue bar, CD90$^+$; blue bar, EpCAM$^-$ CD90$^-$ CD133$^-$. (D) Hierarchical cluster analysis based on 1,561 EpCAM/CD90/CD133-coregulated genes in 172 HCC cases. Each cell in the matrix represents the expression level of a gene in an individual sample. Red and green cells depict high and low expression levels, respectively, as indicated by the scale bar. (E) Pathway analysis of EpCAM/CD90/CD133-coregulated genes. Canonical signaling pathways activated in cluster A (red bar), cluster B (orange bar), or cluster C (light blue bar) with statistical significance ($P$ < 0.01) are shown. (F) Expression patterns of representative genes differentially expressed in EpCAM/CD90/CD133 HCC subtypes. Red bar, EpCAM$^+$; orange bar, CD133$^+$; light blue bar, CD90$^+$; blue bar, EpCAM$^-$ CD133$^-$ CD90$^-$.

**Table 2. Tumorigenic Capacity of Unsorted, EpCAM+, EpCAM−, CD90+, and CD90− Cells From Primary HCCs and Xenografts**

| Sample | CD133 (%) | CD90 (%) | EpCAM (%) | Cell Surface Marker | Number of Cells | Tumor Formation 2M | 3M |
|---|---|---|---|---|---|---|---|
| P1 | 0 | 3.1 | 0 | Unsorted | $1 \times 10^7$ | 0/5 | 0/5 |
| | | | | CD90+ | $1 \times 10^5$ | 0/5 | 0/5 |
| | | | | CD90− | $1 \times 10^5$ | 0/5 | 0/5 |
| P2 | 0.06 | 7.0 | 0.06 | Unsorted | $1 \times 10^7$ | 0/5 | 0/5 |
| | | | | CD90+ | $1 \times 10^5$ | 0/5 | 0/5 |
| | | | | CD90− | $1 \times 10^5$ | 0/5 | 0/5 |
| P3 | 0 | 1.3 | 0 | Unsorted | $1 \times 10^6$ | 0/2 | 0/2 |
| | | | | CD90+ | $1 \times 10^4$ | 0/4 | 0/4 |
| | | | | CD90− | $1 \times 10^4$ | 0/4 | 0/4 |
| P4 | 0 | 0.6 | 17.5 | Unsorted | $1 \times 10^6$ | 3/4 | 4/4 |
| | | | | EpCAM+ | $1 \times 10^3$ | 0/3 | 2/3 |
| | | | | | $1 \times 10^4$ | 3/4 | 4/4 |
| | | | | | $1 \times 10^5$ | 3/3 | 3/3 |
| | | | | CD90+ | $1 \times 10^3$ | 0/3 | 0/3 |
| | | | | | $1 \times 10^4$ | 0/4 | 0/4 |
| | | | | | $1 \times 10^5$ | 0/3 | 0/3 |
| | | | | EpCAM− CD90− | $1 \times 10^3$ | 0/3 | 0/3 |
| | | | | | $1 \times 10^4$ | 0/4 | 0/4 |
| | | | | | $1 \times 10^5$ | 0/3 | 0/3 |
| P5 | 0 | 0.8 | 29.7 | Unsorted | $1 \times 10^6$ | 0/5 | 0/5 |
| | | | | EpCAM+ | $1 \times 10^5$ | 0/5 | 0/5 |
| | | | | CD90+ | $1 \times 10^5$ | 0/5 | 0/5 |
| | | | | EpCAM− CD90− | $1 \times 10^5$ | 0/5 | 0/5 |
| P6 | 0 | 0.7 | 0 | Unsorted | $1 \times 10^6$ | 0/2 | 0/2 |
| | | | | CD90+ | $1 \times 10^4$ | 0/4 | 0/4 |
| | | | | CD90− | $1 \times 10^4$ | 0/4 | 0/4 |
| P7 | 1.38 | 4.5 | 4.4 | Unsorted | $1 \times 10^6$ | 2/2 | 2/2 |
| | | | | EpCAM+ | $2 \times 10^2$ | 0/3 | 0/3 |
| | | | | | $1 \times 10^3$ | 0/3 | 1/3 |
| | | | | | $1 \times 10^4$ | 2/4 | 4/4 |
| | | | | CD90+ | $2 \times 10^2$ | 0/3 | 0/3 |
| | | | | | $1 \times 10^3$ | 0/3 | 0/3 |
| | | | | | $1 \times 10^4$ | 0/4 | 0/4 |
| | | | | EpCAM− CD90− | $1 \times 10^3$ | 0/3 | 0/3 |
| | | | | | $1 \times 10^4$ | 0/3 | 0/3 |
| | | | | | $1 \times 10^5$ | 0/4 | 0/4 |
| P8 | 0 | 0.08 | 0 | Unsorted | $1 \times 10^5$ | 0/4 | 0/4 |
| | | | | CD90+ | $1 \times 10^3$ | 0/3 | 0/3 |
| | | | | CD90− | $1 \times 10^5$ | 0/3 | 0/3 |
| P9 | 0 | 0.26 | 0 | Unsorted | $1 \times 10^5$ | 0/4 | 0/4 |
| | | | | CD90+ | $1 \times 10^3$ | 0/3 | 0/3 |
| | | | | CD90− | $1 \times 10^5$ | 0/3 | 0/3 |
| P10 | 0 | 0.78 | 0 | Unsorted | $1 \times 10^4$ | 0/4 | 0/4 |
| | | | | CD90+ | $1 \times 10^3$ | 0/3 | 0/3 |
| | | | | CD90− | $1 \times 10^4$ | 0/3 | 0/3 |
| P11 | 0 | 0.1 | 1.54 | Unsorted | $5 \times 10^4$ | 0/2 | 0/2 |
| | | | | EpCAM+ | $1 \times 10^3$ | 0/3 | 0/3 |
| | | | | CD90+ | $1 \times 10^3$ | 0/3 | 0/3 |
| | | | | EpCAM− CD90− | $1 \times 10^4$ | 0/3 | 0/3 |
| P12 | 0.06 | 0.05 | 0.09 | Unsorted | $1 \times 10^5$ | 0/3 | 3/3 |
| | | | | CD90+ | $1 \times 10^3$ | 0/4 | 1/4 |
| | | | | CD90− | $1 \times 10^3$ | 0/4 | 1/4 |
| | | | | | $1 \times 10^4$ | 0/3 | 3/3 |

(Continued)

**TABLE 2. (Continued)**

| Sample | CD133 (%) | CD90 (%) | EpCAM (%) | Cell Surface Marker | Number of Cells | Tumor Formation 2M | 3M |
|---|---|---|---|---|---|---|---|
| P13 | 0 | 0.03 | 67.7 | EpCAM+ | $5 \times 10^5$ | 4/4 | NA |
| | | | | | $5 \times 10^4$ | 3/3 | NA |
| | | | | | $5 \times 10^3$ | 3/3 | NA |
| | | | | EpCAM− | $5 \times 10^5$ | 0/4 | NA |
| | | | | | $5 \times 10^4$ | 0/3 | NA |
| | | | | | $5 \times 10^3$ | 0/3 | NA |
| P14 | 24.0 | 0.06 | 3.1 | EpCAM+ | $5 \times 10^3$ | 4/5 | NA |
| | | | | EpCAM− | $5 \times 10^3$ | 2/5 | NA |
| P15 | 0 | 2.45 | 0 | CD90+ | $5 \times 10^4$ | 3/4 | NA |
| | | | | | $5 \times 10^3$ | 1/3 | NA |
| | | | | | $5 \times 10^2$ | 1/3 | NA |
| | | | | CD90− | $5 \times 10^4$ | 2/4 | NA |
| | | | | | $5 \times 10^3$ | 1/3 | NA |
| | | | | | $5 \times 10^2$ | 0/3 | NA |

NA, not available.

contained definite CD133+ cells (20%) (Table 2). CD90+ cells were detected at variable frequencies in all 15 HCCs analyzed.

To explore the status of these CSC marker-positive cells in HCC in a large cohort, we utilized oligo-DNA microarray data from 238 HCC cases (GEO accession no.: GSE5975) to evaluate the expression of *EPCAM* (encoding EpCAM and CD326), *THY1* (encoding CD90), and *PROM1* (encoding CD133) in whole HCC tissues and nontumor (NT) tissues. Because previous studies demonstrated that CD133+ and CD90+ cells were detected at low frequency (~13.6% by CD133 staining and ~6.2% by CD90 staining) in HCC, but were almost nonexistent in NT liver (4, 5),[4,5] we utilized tumor/nontumor (T/N) gene-expression ratios to detect the existence of marker-positive CSCs in tumor. Accordingly, we showed that a 2-fold cutoff of T/N ratios of *EPCAM* successfully stratifies HCC samples with EpCAM+ liver CSCs.[9,10]

A total of 95 (39.9%), 110 (46.2%), and 31 (13.0%) of the 238 HCC cases were thus regarded as EpCAM+, CD90+, and CD133+ HCCs (T/N ratios: ≥2.0), respectively. As observed in the FACS data described above, we detected coexpression of EpCAM and CD90 in 45 HCCs (18.9%), EpCAM and CD133 in five HCCs (2%), CD90 and CD133 in five HCCs (2%), and EpCAM, CD90, and CD133 in 11 HCCs (4.6%). To clarify the characteristics of gene-expression signatures specific to stem cell marker expression status, we selected 172 HCC cases expressing a single CSC marker (34 EpCAM+ CD90− CD133−, 49 EpCAM− CD90+ CD133−, and 10 EpCAM− CD90− CD133+) or all marker-negative HCCs (79 EpCAM− CD90− CD133−). A class-comparison analysis with

univariate F tests and a global permutation test (×10,000) yielded a total of 1,561 differentially expressed genes. Multidimensional scaling (MDS) analysis using this gene set indicated that HCC specimens were clustered in specific groups with statistical significance ($P < 0.001$). Close examination of MDS plots revealed three major HCC subtype clusters: all marker-negative HCCs (blue spheres); EpCAM single-positive HCCs (red spheres); and CD90 single-positive HCCs (light blue spheres). CD133$^+$ HCCs (orange spheres) were rare, relatively scattered, and not clustered (Fig. 1B).

We examined the expression of representative hepatic stem/progenitor cell markers AFP, KRT19, and DLK1 in HCCs with regard to the gene-expression status of each CSC marker (Fig. 1C). All three markers were up-regulated in EpCAM$^+$ and CD133$^+$ HCCs, compared with all marker-negative HCCs, consistent with previous findings.[10,11] However, we found no significant overexpression of AFP, KRT19, and DLK1 in CD90$^+$ and all marker-negative HCCs.

Hierarchical cluster analyses revealed three main gene clusters that were up-regulated in EpCAM$^+$ HCCs (cluster A, 706 genes), EpCAM$^+$ or CD133$^+$ HCCs (cluster B, 530 genes), and CD90$^+$ or CD133$^+$ HCCs (cluster C, 325 genes) (Fig. 1D). Pathway analysis indicated that the enriched genes in cluster A (red bar) were associated with chromatin modification, cell-cycle regulation, and Wnt/$\beta$-catenin signaling (Fig. 1E). Genes associated with messenger RNA processing were enriched in clusters A (red bar) and B (orange bar). Surprisingly, genes in cluster C were significantly associated with pathways involved in blood-vessel morphogenesis, angiogenesis, neurogenesis, and epithelial mesenchymal transition (EMT) (light blue bar). Close examination of genes in each cluster suggested that known hepatic transcription factors (FOXA1), Wnt regulators (TCF7L2 and DKK1), and a hepatic stem cell marker (CD24) were dominantly up-regulated in EpCAM$^+$ and CD133$^+$ HCCs (Fig. 1F). By contrast, genes associated with blood-vessel morphogenesis (TIE1 and FLT1), EMT (TGFB1), and neurogenesis (NES) were activated dominantly in CD90$^+$ HCCs and CD133$^+$ HCCs.

**CD90$^+$ HCC Cells Share Features With Mesenchymal Vascular Endothelial Cells.** Because CD133$^+$ HCCs were relatively rare and constituted only 13% (microarray cohort) to 20% (FACS cohort) of all HCC samples analyzed, we focused on the characterization of EpCAM and CD90. To clarify the cell identity of EpCAM$^+$ or CD90$^+$ cells in primary HCCs, we performed IHC analysis of 18 needle-biopsy

specimens of premalignant dysplastic nodules (DNs), 102 surgically resected HCCs, and corresponding NT liver tissues. When examining the expression of EpCAM and CD90 in cirrhotic liver tissue by double-color IHC analysis, we found that EpCAM$^+$ cells and CD90$^+$ cells were distinctively located and not colocalized (Supporting Fig. 1A). Immunoreactivity (IR) to anti-CD90 antibodies (Abs) was detected in vascular endothelial cells (VECs), inflammatory cells, fibroblasts, and neurons, but not in hepatocytes or cholangiocytes, in the cirrhotic liver (Supporting Fig. 1B, panels a,b). IR to anti-EpCAM Abs was detected in hepatic progenitors adjacent to the periportal area and bile duct epithelial cells in liver cirrhosis (Supporting Fig. 1B, panels c,d).

IR to anti-EpCAM Abs was detected in 37 of 102 surgically resected HCCs (Fig. 2A, panel b), but not in 18 DNs (Fig. 2A, panel a). By contrast, no tumor epithelial cells (TECs) showing IR to anti-CD90 Abs were found in any of the 18 DNs or 102 HCCs examined (Fig. 2A, panels c,d). However, we identified CD90$^+$ cells that were morphologically similar to VECs or fibroblasts within the tumor nodule in 37 of the 102 surgically resected HCC tissues ($\geq$5% positive staining in a given area). IR to anti-CD90 Abs was also detected in hepatic mesenchymal tumors (Supporting Fig. 1C, panels a-c), indicating that CD90 is also a marker of liver stromal tumors.

Double-color IHC and immunofluorescence (IF) analysis confirmed the distinct expression of EpCAM and CD90 in HCC (Fig. 2B), consistent with the FACS data (Fig. 1A). Quantitative real-time polymerase chain reaction (qPCR) analysis of sorted EpCAM$^+$, CD90$^+$, and EpCAM$^-$ CD90$^-$ cells after CD45$^+$ cell depletion indicated that the hepatic stem/progenitor markers, AFP and KRT19, were up-regulated in EpCAM$^+$ cells (red bar), whereas the mesenchymal markers, KIT and FLT1, were up-regulated in CD90$^+$ cells (orange bar), compared with EpCAM$^-$ CD90$^-$ cells (blue bar) (Fig. 2C). The hepatocyte marker, CYP3A4, was down-regulated in EpCAM$^+$ cells and not detected in CD90$^+$ cells, compared with EpCAM$^-$ CD90$^-$ cells. POU5F1 and BMI1 were equally up-regulated in both EpCAM$^+$ and CD90$^+$ cells, compared with EpCAM$^-$ CD90$^-$ cells.

EpCAM and CD90 were independently and distinctively expressed in different cellular lineages, so we evaluated the staining of EpCAM and CD90 separately and analyzed the clinicopathological characteristics of surgically resected HCC cases. HCCs were regarded marker positive if $\geq$5% positive staining was detected in a given area. The existence of EpCAM$^+$
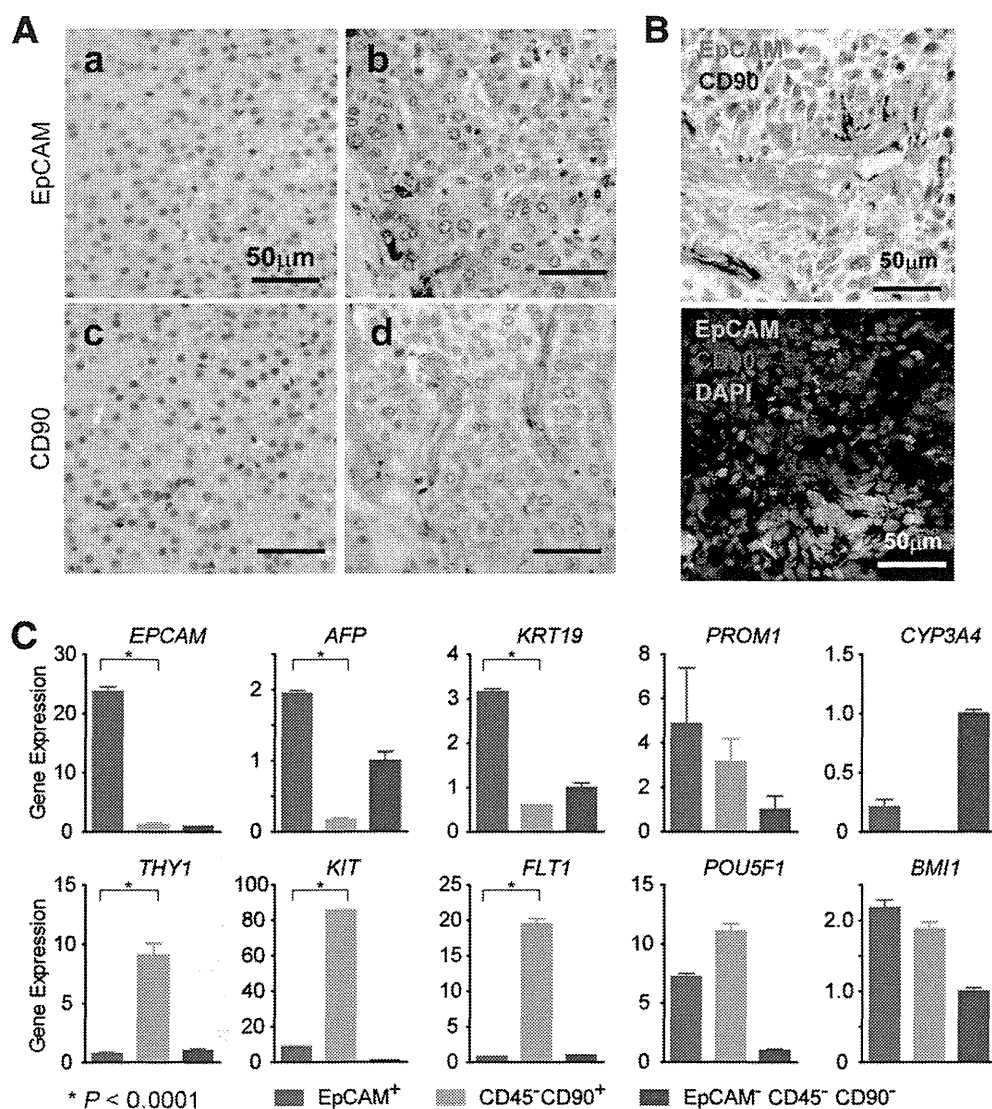
Fig. 2. Distinct EpCAM$^+$ and CD90$^+$ cell populations in HCC. (A) Representative images of EpCAM and CD90 staining in dysplastic nodule (panels a,c) and HCC (panels b,d) by IHC analysis (scale bar, 50 $\mu$m). EpCAM (panels a,b) and CD90 (panels c,d) immunostaining is depicted. (B) Upper panel: representative images of EpCAM (red) and CD90 (brown) double staining in HCC by IHC (scale bar, 50 $\mu$m). Lower panel: representative images of EpCAM (green) and CD90 (red) staining with 4'6-diamidino-phenylindole (DAPI) (blue) in HCC by IF (scale bar, 50 $\mu$m). (C) qPCR analysis of sorted EpCAM$^+$ (red bar), CD90$^+$ (orange bar), or EpCAM$^-$ CD90$^-$ (blue bar) derived from a representative primary HCC. Experiments were performed in triplicate, and data are shown as mean ± standard error of the mean.

cells ($\geq$5%) was characterized by poorly differentiated morphology and high serum AFP values with a tendency for portal vein invasion, whereas the existence of CD90$^+$ cells ($\geq$5%) was associated with poorly differentiated morphology and a tendency for large tumor size (Supporting Tables 2 and 3). Notably, the existence of CD90$^+$ cells was associated with a high incidence of distant organ metastasis, including lung, bone, and adrenal gland, within 2 years after surgery, whereas EpCAM$^+$ cell abundance appeared unrelated to distant organ metastasis.

We evaluated the characteristics of EpCAM$^+$ or CD90$^+$ cells in seven representative HCC cell lines. Morphologically, all EpCAM$^+$ cell lines (HuH1, HuH7, and Hep3B) showed a polygonal, epithelial cell shape, whereas three of four CD90$^+$ cell lines (HLE, HLF, and SK-Hep-1) showed a spindle cell shape (Fig. 3A). EpCAM$^+$ cells were detected in 11.5%, 57.7%, and 99.6% of sorted HuH1, HuH7,

and Hep3B cells, respectively. A small CD90$^+$ cell population (0.66%) was observed in PLC/PRL/5, whereas 91.3%, 10.8%, and 59.0% of CD90$^+$ cells were detected in HLE, HLF, and SK-Hep-1, respectively. Compared with primary HCCs, only EpCAM$^+$ or CD90$^+$ cells were detected in liver cancer cell lines under normal culture conditions (Fig. 3B), suggesting that these cell lines contain a relatively pure cell population most likely obtained by clonal selection through the establishment process.

A class-comparison analysis with univariate $t$ tests and a global permutation test ($\times$10,000) of microarray data yielded two main gene clusters up-regulated in EpCAM$^+$ cell lines (HuH1, HuH7, and Hep3B) (cluster I, 524 genes) or in CD90$^+$ cell lines (HLE, HLF, and SK-Hep-1) (cluster II, 366 genes) (Fig. 3C). PLC/PRL/5 showed intermediate gene-expression patterns between EpCAM$^+$ and CD90$^+$ cell lines using this gene set. Pathway analysis indicated that the genes